SANDIA REPORT
SAND97–1995 • UC–506
Unlimited Release
Printed August 1997

Elements of a Continuous-Wave Borehole Radar

Thurlow W. H. Caffey

Prepared by
Sandia National Laboratories
Albuquerque, New Mexico 87185 and Livermore, California 94550

Sandia is a multiprogram laboratory operated by Sandia Corporation, a Lockheed Martin Company, for the United States Department of Energy under Contract DE-AC04-94AL85000.

Sandia National Laboratories

SF2900Q(8-81)

Issued by Sandia National Laboratories, operated for the United States Department of Energy by Sandia Corporation.

Available to DOE and DOE contractors from
Office of Scientific and Technical Information
P.O. Box 62
Oak Ridge, TN 37831

Prices available from (615) 576-8401, FTS 626-8401

Available to the public from
National Technical Information Service
U.S. Department of Commerce
5285 Port Royal Rd
Springfield, VA 22161

NTIS price codes
Printed copy: A03
Microfiche copy: A01

SAND97-1995
Unlimited Release
Printed August 1997

Distribution
Category UC-506

Elements of a Continuous-Wave Borehole Radar

Final Report
Cooperative Research and Development Agreement SC93-01158
between Sandia National Laboratories
and
Raton Technology Research, Inc., Raton, NM
(formerly RIMtech/Stolar, Inc.)
DOE TTP Number 93-SANL-078-C1
1 March 1993 - 25 April 1996

Thurlow W. H. Caffey
Geophysical Technology Department
Sandia National Laboratories
P. O. Box 5800
Albuquerque, NM 87185-0705

Abstract

The theory is developed for the antenna array for a proposed continuous-wave, ground-penetrating radar for use in a borehole, and field measurements are presented. Accomplishments include the underground measurement of the transmitting beam in the azimuth plane, active azimuth-steering of the transmitting beam, and the development of a range-to-target algorithm. The excellent performance of the antenna array supports the concept of a continuous-wave borehole radar. A field-prototype should be developed for use in both geothermal zones and for the exploration and recovery of oil and gas.

Acknowledgment

I wish to thank Eugene F. Roseth, Department 6525, who served as project leader for all but the last three weeks of this effort, for his many contributions. Larry Anderson, Department 9573, performed both mechanical and electrical design, layout, fabrication, and assembly. Jack Bartberger, Department 5736, devised the dielectric, four-bow, centering devices which eliminated a serious problem.

Contents

Apparatus

Field Measurements

Figures

Elements of a Continuous-Wave Borehole Radar

Preface

This project was created to develop, field-demonstrate, and produce a new type of borehole radar, or 'BHR', together with appropriate signal processing to serve the needs of both environmental remediation and the needs of the oil, gas, and geothermal industries. The novel feature of the BHR is the use of continuous-wave transmission that will allow operation in geologic media which are unsuitable for the application of pulse-type borehole radars.

Raton Technology Research, or RTR, the industrial partner under the CRADA, was to assume responsibility for the system design, mechanical package design and construction, general electronic design, receiver construction, final fabrication, and commercial introduction. Sandia was to perform antenna design, target modeling, and development of inversion algorithms. Both partners were to collaborate in the general prototype design, subsystem design and testing, development of operational software, and the conduct of field tests.

All of the technology developed by Sandia was transferred to RTR as required by the CRADA agreement.

This report describes only the design and field work done by Sandia in the areas of antennas, transmitter and receiver electronics, electromagnetic modeling, and range-to-target algorithms. RTR should be contacted for a description of their contributions.

Introduction

The electromagnetic, or 'EM', instruments which may be used in a borehole can be divided into two classes according to the means by which the EM-fields are introduced into the geologic media, namely by direct, physical contact with electrodes or by contact-less methods. The last class establishes the fields either by induction, such as resistivity tools, or by propagation, such as borehole radars. Commercially available induction tools generally operate at frequencies of 200kHz or less, while commercially available borehole radars are generally used at 20MHz or greater. The dearth of commercially available EM borehole instruments between 200kHz and 20MHz is not only a frequency-niche, but is an opportunity worthy of examination.

Niche for Continuous-Wave Radar

Induction tools are usually designed to examine the volume of material relatively near the borehole with use of several multi-turn coils for both transmission and reception. A component of the *magnetic* field links the coil system, in part, by paths in the surrounding earth. The use of a low frequency allows a useful penetration distance into the earth, but higher frequencies are desirable for greater resolution. However, as the frequency is increased, the penetration of the fields into the earth diminishes due to the conductivity of media, and the investigated volume becomes a relatively small zone near the borehole. An upper frequency of about 200kHz is a practical economic choice which satisfies the present commercial market.

Existing borehole radars, or BHRs, are operated in a pulsed mode. Usually, the transmitting antenna is an electric dipole which is especially designed to minimize reflections back into the transmitter. The antenna is both coaxial with the instrument axis and parallel to the borehole centerline. The receiving antennas are usually electric dipole(s) also. They are offset-located along the axis from the transmitting antenna, and may be either parallel to, or coaxial with, the instrument axis. This means that the *electric*-field component parallel to the instrument axis is the component whose reflection is observed. The transmitting antenna is periodically excited by a brief pulse of current where the time period between pulses is usually much greater than the duration of a pulse. During the application of the current-pulse, the receiver amplifier(s) are turned-off to avoid damage. The periodic succession of pulses generates fields, not at a single frequency, but as a band, or, extensive collection, of frequencies. The extent of the frequency-band, and its mean frequency depends, in a complicated manner, on the ratio of the pulse duration to the time period between pulses. The frequency of operation usually refers to the mean frequency.

The pulse radar depends on the expectation that the electromagnetic wave will *propagate*, rather than *diffuse*, along the two-way path through the media to and from the target. This condition must be met in order that a discernible return pulse can be observed at the receiver output, and requires that the Loss Tangent of the media be much less than unity.

The Loss Tangent is a dimensionless ratio , and is related to the electrical parameters of the media by:

$$g = \text{Loss Tangent} = \frac{\sigma}{\omega \varepsilon_o \varepsilon_r}, \qquad (1)$$

where

σ = Conductivity of the media, Siemens/meter; 1E-4 $\leq \sigma \leq$ 4 S/m;

ε_o = Dielectric constant of free-space, about 8.85419E-12 Farads/meter;

ε_r = Relative dielectric constant, RDC, of the media; $1 \leq \varepsilon_r \leq 81$;

and

$\omega = 2\pi \bullet$frequency(Hertz), radians/second.

The inverse relation of the Loss Tangent to frequency effectively establishes a lower frequency limit for a particular choice of media parameters.

The 'frequency niche' is actually a 'frequency *and* media' niche which is set by the combined effect of both frequency and the media parameters upon two different operational concepts. The combined effect limits the upper operating frequency of induction tools and the lower operating frequency of pulse-type BHRs. The continuous-wave BHR readily operates over a wide range of media parameters at frequencies above that of induction tools and below that of pulse-type BHRs. The experimental work reported herein, for example, was performed at 1MHz.

In a continuous-wave BHR there will be direct communication between the transmitter and the receiver(s) both within the instrument package and within the interior of the borehole. This 'self-clutter' must be minimized by the choice of antennas so that the returned signal due to the geologic media can be detected. This most fundamental choice in the system concept is described next.

Antenna Choices

The choice of antennas is limited at continuous frequencies below 20MHz to elementary dipoles, either electric or magnetic. Because of the cylindrical shape of a borehole, it is desirable that at least one antenna take advantage of the available length parallel to the borehole axis. The transmitting antenna may be either electric or magnetic dipole, and each may be oriented either parallel or transversely to the borehole axis. There are the same four choices of receiving antennas for each choice of transmitting antenna, so there are sixteen possible choices to discuss.

Transverse electric dipole. An electric dipole, transverse to the axis, is excluded because its length would be limited by the inner diameter of the instrument package. Both the transmitting moment and the received open-circuit voltage are proportional to the length of an electric dipole, and it is unfavorable to consider a transverse electric dipole by comparison with an electric dipole parallel to the borehole axis.

Parallel electric dipole source. An electric dipole, parallel to the axis, may be given a useful length, but it was excluded as a source because it was anticipated that the capacitance across the gap between the two sections of the dipole would be very small. Consequently, below 20MHz, the impedance presented to the transmitter amplifier would be very great, and a large peak voltage would be required to drive the dipole with the current necessary to generate a useful moment.

Magnetic dipole sources. Only magnetic dipoles remain to be chosen as a source and, of course, they will be within an insulated cylindrical instrument package. There is a substantial theoretical and experimental literature on the properties of an insulated magnetic transmitter, both with and without a ferrite-load. A moderate list would include Wait, 1957; Kraichman, 1962; Hansen, 1963; Moore, 1963; Wait & Spies, 1964; Galejs, 1965; and Smith, 1973. This body of work supports, among other insights, J. R. Wait's 1957-statement that, '*the external fields...are not dependent on the presence of the (insulating) cavity...when the product of the cavity radius and the propagation factor of the surrounding media is less than unity*' which is a basic premise of this work.

I assume that the instrument axis is coincident with the borehole axis which is the Z-axis of a Cartesian system with the positive direction toward the upper end of the borehole. The magnetic sources and the receiving antennas are centered on the Z-axis to minimize crosstalk. The effect of off-setting the antennas from the centerline will be examined later.

Horizontal magnetic dipole source. A dipole with its moment directed along the positive X-axis will be referred to as an 'HMD_X'. It may seem that the inner diameter of the instrument might severely constrain the dipole moment, but this constraint can be reduced by using multiple rectangular turns in which two opposite sides are extended parallel to the instrument axis. The area per turn can be large, but the number of turns will be limited by the cylindrical cross-section of the instrument. The center of the winding should be directly within the YZ-plane so that the winding is symmetrical with respect to the YZ-

plane. An examination of the fields from the HMD_X will indicate which type of receiving dipole to use.

Following *Sommerfeld (1949)*, with suppressed time-dependence as $\exp(-j\omega t)$, where $\omega = 2\pi f$, and 'f' is the operating frequency, the HMD_X generates an magnetic Hertz vector:

$$\bar{\Pi}_X = \frac{IdA}{4\pi R}\exp(jkR) \qquad \text{Ampere-meters,} \quad (2)$$

I = dipole current, at frequency 'f', in peak Amperes;
dA = area of the infinitesimal loop through which 'I' circulates in a counter-clockwise sense as viewed from the positive X-axis, meters^2;
R = spherical radius from the dipole to the field point, meters;
j = $\sqrt{-1}$;
and $k = \alpha + j\beta$, is the propagation factor, meters^{-1}, in which

$$\alpha = \omega\sqrt{\frac{\mu_o\mu_r\varepsilon_o\varepsilon_r}{2}\left(+1+\sqrt{1+g^2}\right)}\ , \text{ is the real part, and}$$

$$\beta = \omega\sqrt{\frac{\mu_o\mu_r\varepsilon_o\varepsilon_r}{2}\left(-1+\sqrt{1+g^2}\right)}\ \text{ is the imaginary part,}$$

in which 'g' is the Loss Tangent defined previously (*Stratton 1941*). The electric and magnetic fields are derived from a magnetic Hertz vector by:

$$E = j\mu\omega\nabla x\bar{\Pi}_X, \qquad \text{peak-Volts/meter;} \quad (3)$$

and

$$H = k^2\bar{\Pi}_X + \nabla\left(\nabla\bullet\bar{\Pi}_X\right), \qquad \text{peak-Amperes/meter.} \quad (4)$$

Consequently, using $M = \frac{IdA}{4\pi}$, the fields are given by:

$$E_X \equiv 0 \qquad (5)$$

$$E_Y = -j\mu_r\mu_o\omega M\cos\theta\left(1-jkR\right)\exp(jkR)/R^2 \qquad (6)$$

$$E_Z = j\mu_r\mu_o\omega M\sin\theta\sin\phi\left(1-jkR\right)\exp(jkR)/R^2 \qquad (7)$$

$$H_X = -M\left\{\left[1-jkR-k^2R^2\right]+\sin^2\theta\cos^2\phi\left[3-j3kR-k^2R^2\right]\right\}\exp(jkR)/R^3 \qquad (8)$$

$$H_Y = M\left\{\sin^2\theta \sin\phi\cos\phi\left[3 - j3kR - k^2R^2\right]\right\}\exp(jkR)/R^3 \qquad (9)$$

$$H_Z = M\left\{\sin^2\theta \cos\theta\cos\phi\left[3 - j3kR - k^2R^2\right]\right\}\exp(jkR)/R^3 \qquad (10)$$

R, θ, and ϕ are the spherical coordinates of distance, polar angle, and azimuth angle; "μ_r" is the relative magnetic permeability, and "μ_o" is the permeability of free space, $4\pi\cdot10^{-7}$ Henries/meter.

The E_Y and E_Z fields are the same except for the trigonometric terms, so E_Y has a relative maxima on the Z-axis, Figure 1, and E_Z has maxima on the Y-axis as shown in Figure 2. The relative magnitudes of both fields are independent of both R and kR. The use of a Y-directed electric dipole as a receiver is impossible because the E_Y- maxima on the Z-axis would strongly couple the receiver to the HMD_X. A Z-directed electric dipole could be used to detect the return E_Z-field, but the dipole must be carefully centered on, and parallel to, the Z-axis to avoid crosstalk.

The use of an X-directed magnetic dipole as a receiver is impossible because the transmitted H_X-component does not have a null along the Z-axis, and the receiver would be strongly coupled to the HMD_X.

The remaining two components, H_Y and H_Z, each have a null along the Z-axis and their relative magnitudes are independent of R and kR. The magnitude of H_Y has four-lobes with maxima along lines which make a 45° angle with the X and Y axis as shown in Figure 3. Each lobe is out of phase with the lobes on either side, so that a Y-directed magnetic dipole could be used as a receiver with minimal coupling to the HMD_X. However, it would be very difficult to interpret the target return when the illuminating radiation has four equal major lobes, so the H_Y-receiver is discarded.

The magnitude of H_Z has four lobes with maxima in the XZ-plane along lines which make an angle of about 54.7° with the positive Z-axis as shown in Figure 4. A Z-directed magnetic dipole could be used as a receiver, but the difficulty of interpreting the target response to four illuminating lobes forces the discard of the H_Z-receiver.

An electric dipole, parallel to the Z-axis, namely a vertical electric dipole or 'VED', is the preferred receiver to use for the HMD_X source.

Vertical magnetic dipole source. A dipole with its moment directed along the positive Z-axis will be referred to as a '*VMD*'. This source is attractive because the turns-area product may be increased easily by winding a multi-turn coil around a form (or a ferrite rod) centered on the Z-axis. The area per turn will be smaller than for an HMD_X, but the number of turns can be greater and the ferrite can greatly increase the H-field *[Rumsey and Weeks, 1956; De Vore and Bohley, 1977]*. The fields of a non-ferrite *VMD* are derived from a magnetic Hertz vector along the Z-axis with these results:

MDEYF03.DCF
MDEYF01.DAT

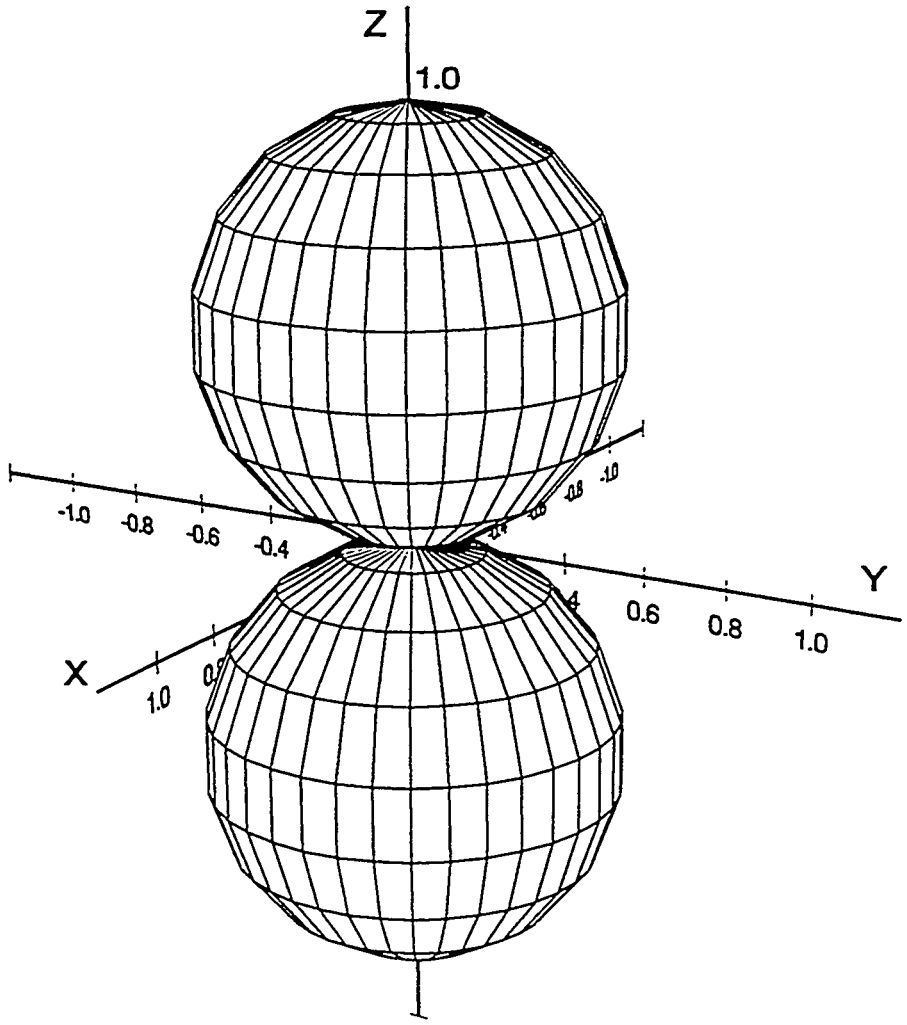

Figure 1
Relative Ey-field from an X-directed magnetic dipole

IMDEZF03.DCF
IMDEZF01.DAT

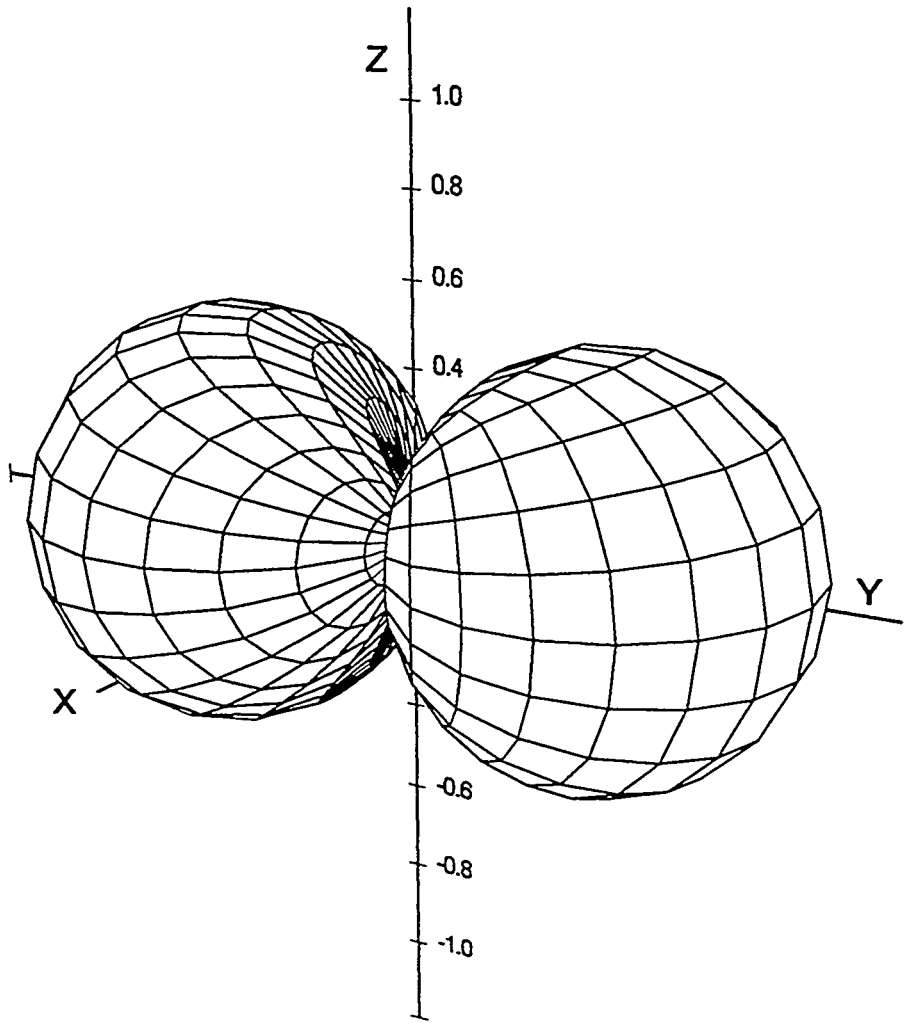

Figure 2
Relative Ez-field from an X-directed magnetic dipole

IMDXHYF.DCF
IMDXHYF.DAT

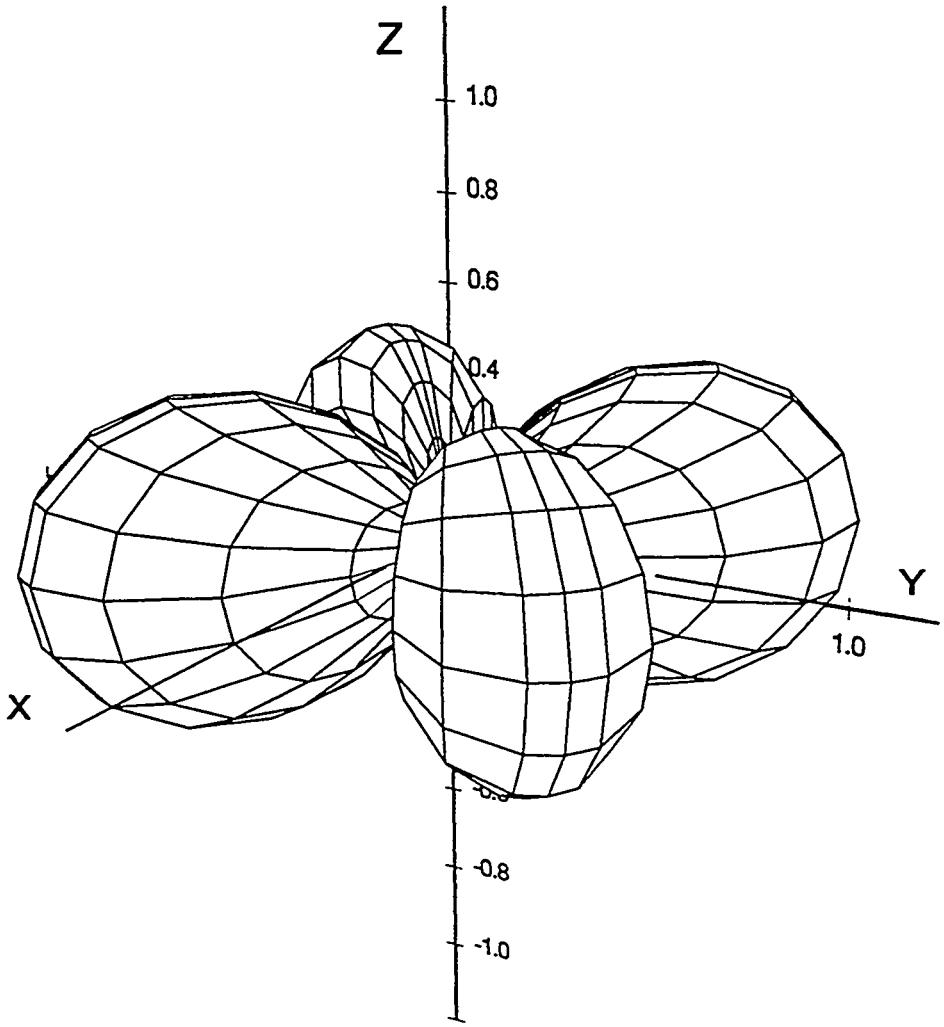

Figure 3
Relative Hy-field from an X-directed magnetic dipole

IMDXHZF.DCF
IMDXHZF.DAT

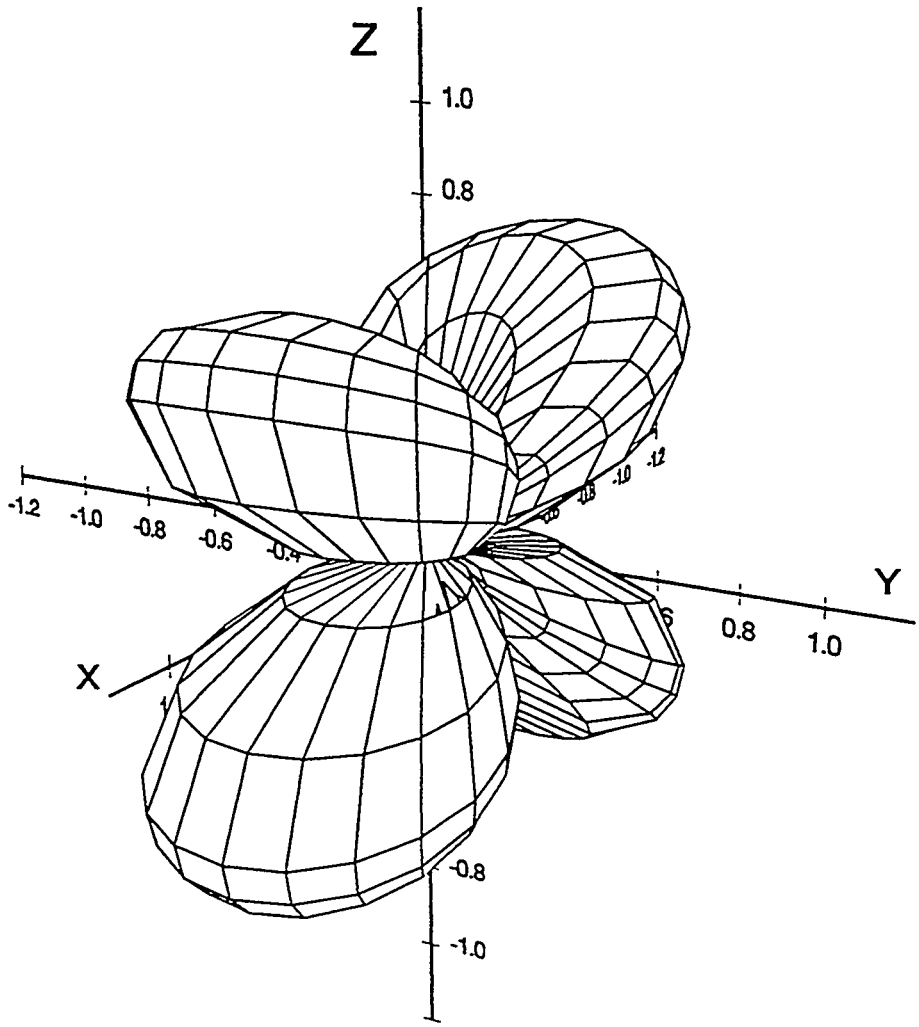

Figure 4
Relative Hz-field from an X-directed magnetic dipole

$$E_X = -j\mu_r\mu_o\omega M \sin\theta \sin\phi\left(1 - jkR\right)\exp(jkR) / R^2 \tag{11}$$

$$E_Y = j\mu_r\mu_o\omega M \sin\theta \cos\phi\left(1 - jkR\right)\exp(jkR) / R^2 \tag{12}$$

$$E_Z \equiv 0 \tag{13}$$

$$H_X = M\left\{\sin\theta\cos\theta\cos\phi\left[3 - j3kR - k^2R^2\right]\right\}\exp(jkR) / R^3 \tag{14}$$

$$H_Y = M\left\{\sin\theta\cos\theta\sin\phi\left[3 - j3kR - k^2R^2\right]\right\}\exp(jkR) / R^3 \tag{15}$$

$$H_Z = M\left\{\left[1 - jkR - k^2R^2\right] + \cos^2\theta\left[3 - jkR - k^2R^2\right]\right\}\exp(jkR) / R^3 \tag{16}$$

Here the E_X and E_Y fields have a null along the Z-axis and are bi-lobed with maxima along the Y- axis and X-axis respectively. However, the length of the receiving dipoles will be limited by the instrument diameter, and will be less than the dipole-length used to receive the E_Z-field from the HMD_X. Both of the E-fields from the VMD could be received and recorded simultaneously, but detection will be less sensitive than detection of the E_Z-field from the HMD_X.

Both the H_X and H_Y fields have a null along the Z-axis, but they each have four-lobes as shown in Figures 5 and 6. These lobes, located in the XZ-plane and YZ-plane respectively, will confound interpretation and their possible use is discarded.

The use of a Z-directed magnetic dipole as a receiver is impossible because the H_Z-field is a maximum on the Z-axis, and the receiver cannot be de-coupled from the VMD source.

Only the E_X and E_Y fields from the VMD have a bi-lobed structure, and electric dipoles parallel to the X and Y axis would be the most appropriate receivers for the VMD source.

Antenna Array. There are two candidates for a choice of transmitter/receiver-array, and the choice will be based on crosstalk-susceptibility and target application.

If the target features are thought to be extended parallel to the borehole axis, such as vertical fissures, the E_Z-field from an HMD_X should be used. However, if the target features are extended perpendicular to the borehole axis, the use of the E_X and E_Y fields from a *VMD* would be preferable.

Because a *VMD* can be ferrite-loaded, the E_X and E_Y fields can be increased to overcome the fact that the length of the X and Y receiving dipoles will be shorter than the E_Z-dipole used with the HMD_X-transmitter. However, the receiver electronics and batteries can be placed entirely within the metal walls of the E_Z-dipole which greatly reduces crosstalk-

/MDHXF.DCF
/MDHXF.DAT

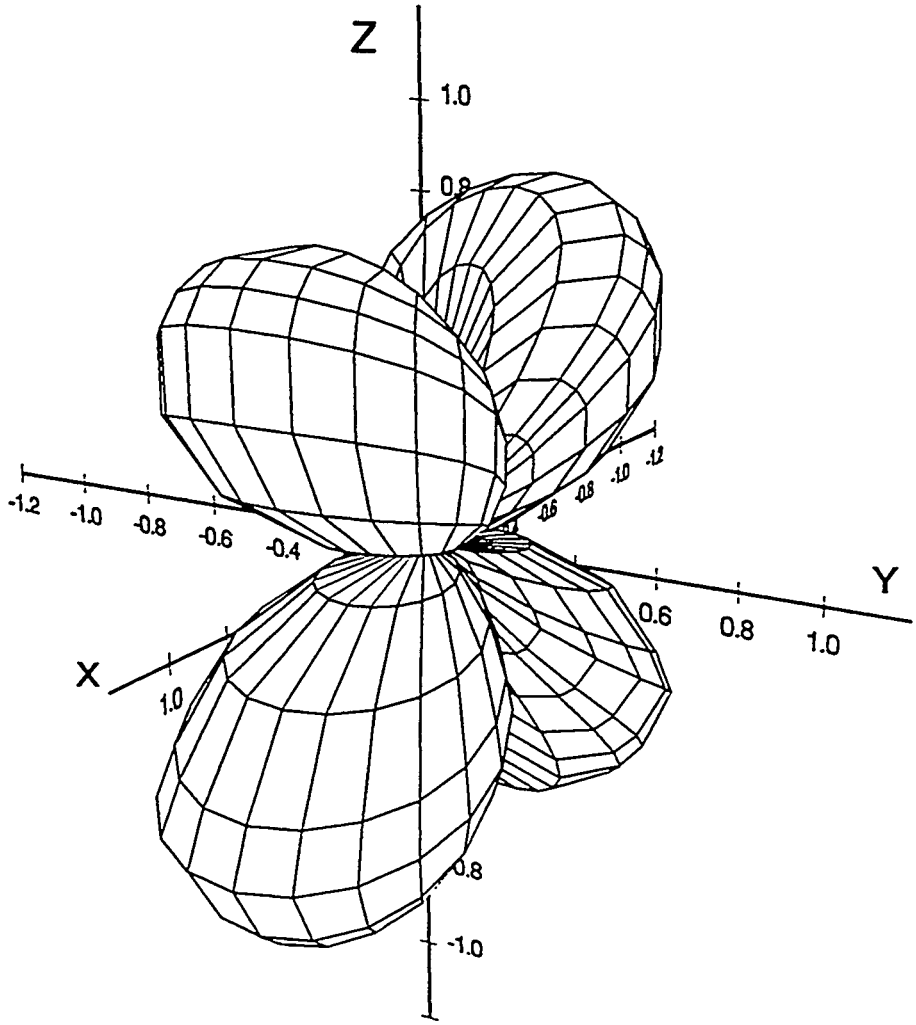

Figure 5
Relative Hx-field from a Z-directed magnetic dipole

VMDHYF.DCF
VMDHYF.DAT

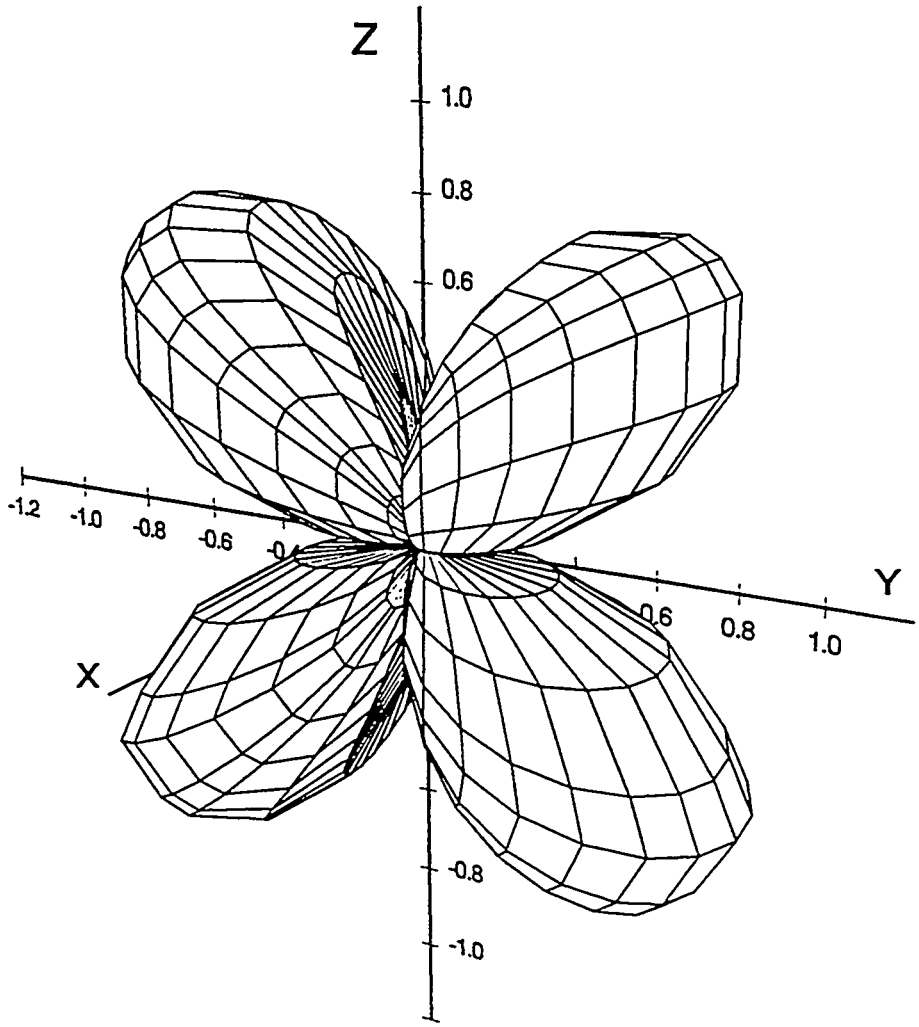

Figure 6
Relative Hy-field from a Z-directed magnetic dipole

susceptibility to the HMD_X. There is no such protective advantage for the receiving E_X and E_Y dipoles for the VMD whose crosstalk fields will be stronger than for the HMD_X-transmitter because of the ferrite-load.

Our primary targets were fissures parallel to the borehole, and the HMD_X-transmitter was chosen for subsequent development.

Crosstalk

Direct physical observation, much less measurement, of crosstalk is difficult because all reflection mechanisms outside the instrument must be removed. This is difficult to achieve at 1MHz in air where the wavelength is 300km! Immersion in a large, moderately-conducting body of water would greatly reduce the wavelength, but the cost of a water-tight instrument and field-operations over water discourage this idea. Otherwise, in circumstances when known targets are present, but are not detected, crosstalk must be suspected as a cause.

It is necessary to have the dimensions of the antennas and the separation between them in order to make calculations for crosstalk, and this information follows next.

Antenna Construction. The VED is composed of two copper cylindrical tubes, 6.6cm OD by 9.90cm long, with a 0.20cm wall. The tubes are inserted over a fiberglass tube which has a circumferential ridge at the midpoint to serve both as an axial support and to provide a gap of 0.20cm. A Lexan™ polycarbonate tube is interference-fitted over the electrodes both to protect the outer surfaces and to serve as radial spacer to center the VED within a Lexan radome. Figure 7 is a cross-section of the VED assembly in which the gap between the radial spacer and the radome is not shown because the gap is $\leq 100\mu$. All of the receiver electronics, including batteries, are located within the hollow interior of the fiberglass support tube.

The HMD_X is wound rectangularly on a cylindrical form with an area of $0.20m^2$, and carries a current of 0.33 peak Amperes to provide a moment of 0.067 Amperes-m^2. Both the HMD_X and VED antennas are slipped inside the radome together with a hollow spacer-tube to separate them, center-to-center, along the instrument axis by 3.2m.. The worst-case design value of the maximum radial clearance is only 100μ or 0.004 inches. This is a minimal clearance, and talcum powder, in small amounts, was necessary to lubricate the insertion of the antennas. The spacer tube has a smaller radius than the VED and did not require lubrication.

Crosstalk from the HMD_X to the VED will occur whenever any part of the VED is not perfectly coincident with the *Z*-axis. There are two principal ways for non-coincidence to occur, namely by translation and rotation of either or both of the antennas.

Translation. As a worst-case example, if the VED were kept parallel to the *Z*-axis and translated along the *Y*-axis, a non-zero E_Z-field will occur along the antenna as indicated by the increasing magnitude along the *Y*-axis as shown in Fig.2. This field must be sampled around the circumference and integrated over the length of each half of the VED to find the potential of each half. The difference of the two potentials is the open-circuit voltage.

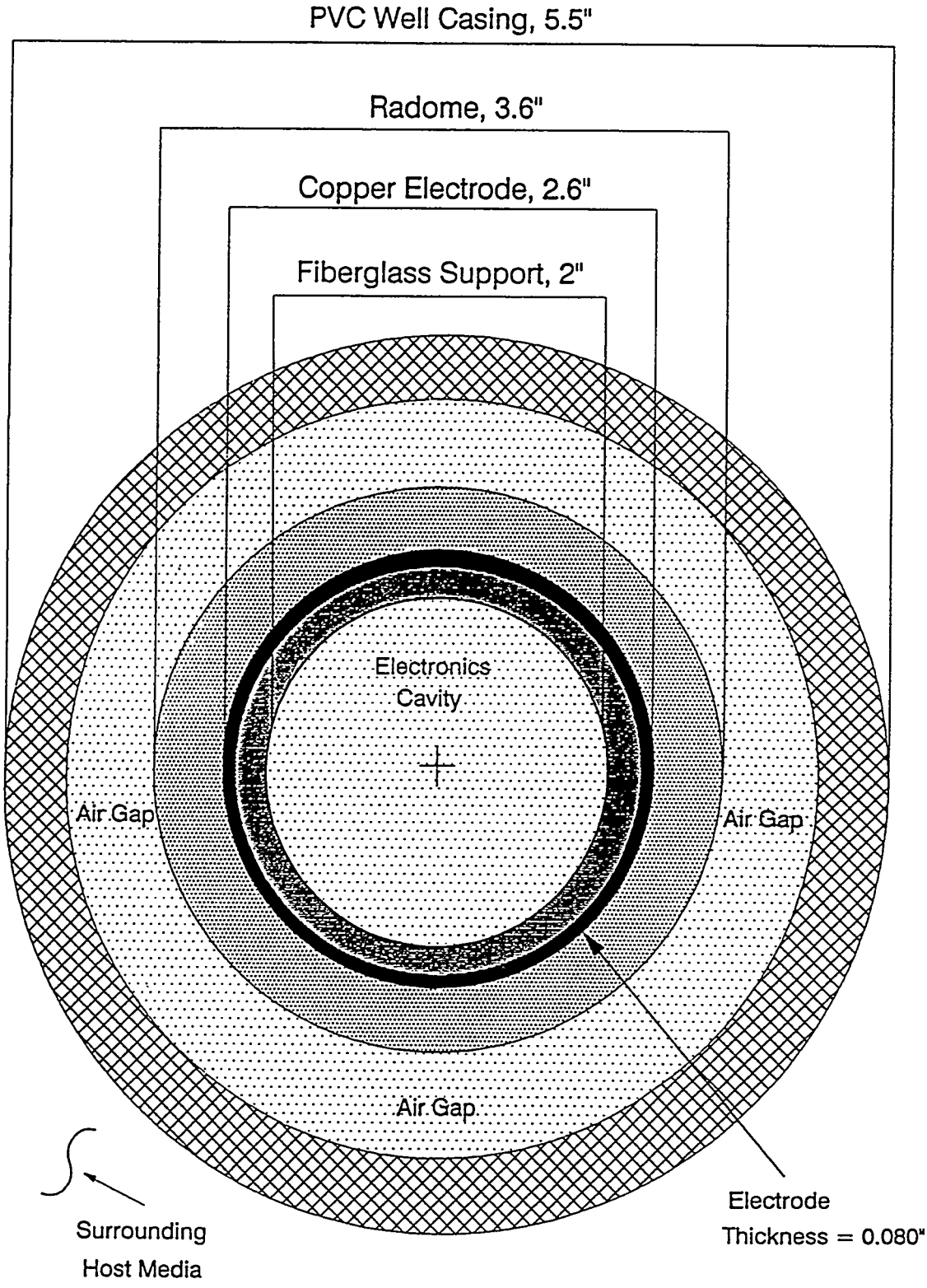

Figure 7

Cross-Section of Receiver in the Well Casing

The potential in each half of the VED was computed by setting the Y-offset to 200μ to allow for possible opposite offsets of the transmitting and receiving antennas. The surface of each half-dipole was divided into 2° increments in azimuth and 0.1cm increments in length. The potential at each incremental surface was computed as the product of the E_Z-field by 0.1cm. These incremental potentials were added and divided by 180 to obtain the potential of each half. The crosstalk was computed as 3.8nVrms for the antennas in air. Because Lexan was used for the radome, the spacer tube, the winding form for the HMD_X, and as a sleeve over the VED itself, the crosstalk was also computed for the antennas encapsulated solidly in Lexan. This material has an RDC of 2.96 and a conductivity of 16.5mS/m at 1MHz. The Lexan crosstalk was computed as 3.5nVrms, which is almost the same as the crosstalk in air.

Rotation. Another crosstalk mechanism is through the E_Y-field if the VED should be inclined by an angle 'η' with respect to the Z-axis. Eq.(6) shows that E_Y is proportional to $\cos\eta$, but the projection of the dipole surface in the Y-direction is proportional to $\sin\eta$. The product, which is necessary for numerical integration, is proportional simply to η for very small rotation angles. The worst effect will occur if the rotation is in the YZ-plane because that is the only circumstance where E_Y will be projected on the entire length of the VED. The HMD_X and the VED may be considered rotated in opposite senses to provide a maximum combined-rotation angle.

The geometry for calculation of the rotation angle is shown in Figure 4 where the instrument package, either HMD_X or VED, is rotated about its midpoint on the instrument centerline. The rotation angle is given by

$$\eta = 90^\circ - (\psi + \xi) \qquad (17)$$

where $\psi = Arc\tan(Width / Length)$, and $\xi = Arc\cos([Width + 2\delta] / Hypoteneuse' D')$. The formula, Eq. (17), requires the difference between two numbers of nearly the same value because η is less than 1°. Both the width and length must be known to a relative accuracy of 10^{-4} to compute η to the nearest 0.01° for the dimensions used in the antenna packages. The measured dimensions predict a worst case rotation angle of 0.06° for which a computer code furnishes a crosstalk of 41nVrms in air and 43nVrms in Lexan. These values are about 12-times the estimates of translation crosstalk, and are so large that they would not have gone unnoticed in our experimental work. Evidently, the singular worst-case of the HMD_X and the VED rotated oppositely and precisely in the YZ-plane did not occur.

Borehole Crosstalk in Media. The foregoing has been based on fields in a homogeneous space and has ignored the effect of the cylindrical walls of the borehole itself. The E_Z-field is tangent to the borehole wall, and will be reflected in part to possibly reach the VED some distance away on the axis, so it is possible that the crosstalk could be increased in the translation case. The E_Y-field is normal to the borehole boundary along the Y-direction and tangential to the boundary along the X-direction, and the effect on rotation-crosstalk

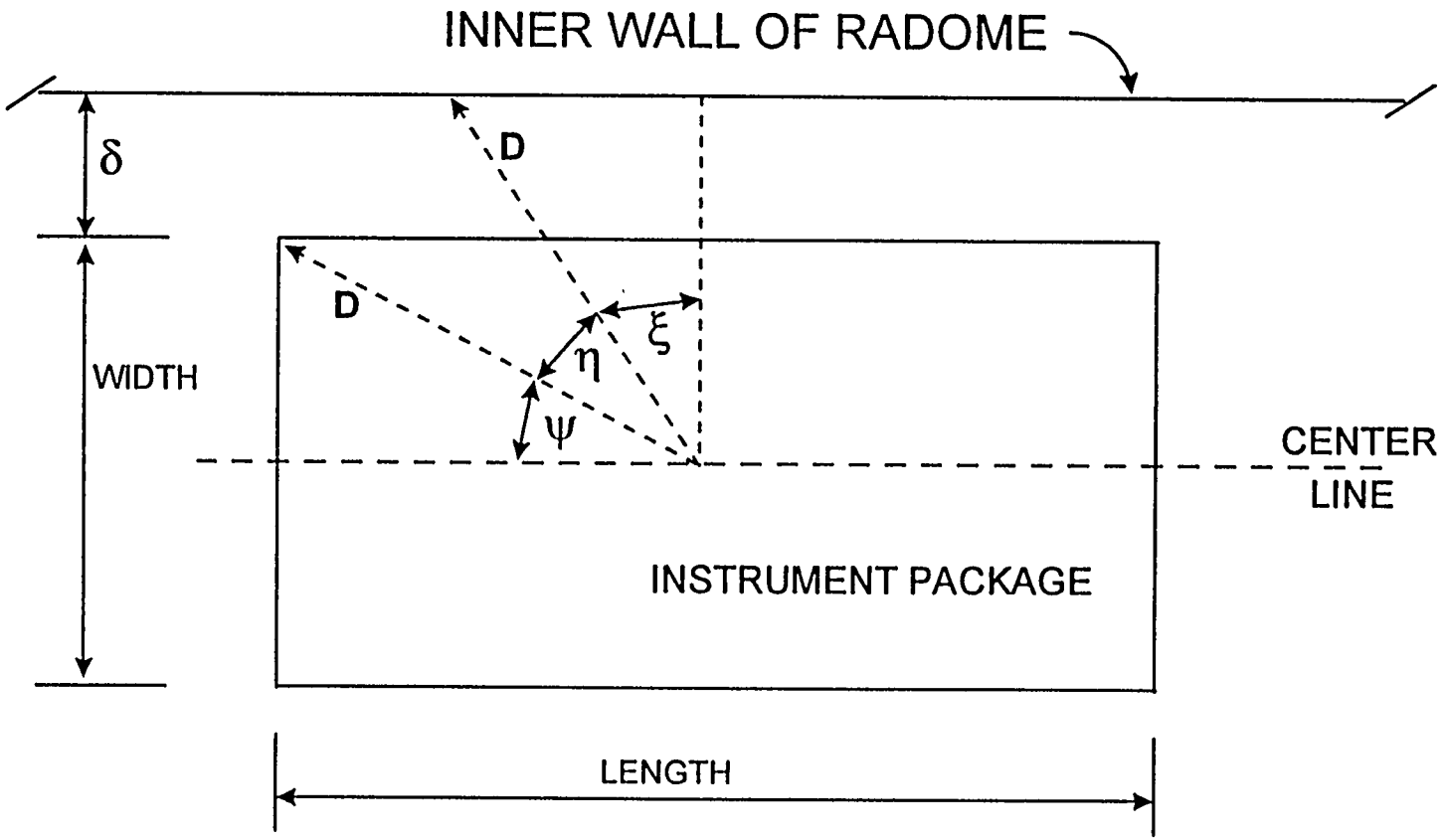

FIGURE 8 TILT GEOMETRY

is not obvious. As an example, however, a very large effect was noted in field experiments when the instrument was not aligned with the borehole axis: When the instrument was translated to the borehole boundary, the output of the receiver increased noticeably. This was solved by using a dielectric, four-arm, centering-bow at each end of the instrument.

Beam-Steering

There are three elements required for a radar: The detection of a target, an estimate of its angular location, and an estimate of the range-to-target. If a borehole radar is traversed along the borehole while sweeping its beam perpendicularly to the axis, a target will be located when a maximum response is observed along a particular azimuth bearing.

A Second HMD. For beam steering we add a second HMD concentric with the first, but with its vector in the *negative* Y-direction to conveniently eliminate a minus sign. The E_Z-field is given by:

$$E_{Z,-Y} = j\mu_r\mu_o\omega M \sin\theta\cos\phi(1 - jkR)\exp(jkR) / R^2 \tag{18}$$

where the 2nd subscript denotes that the HMD is directed along the negative Y-axis. Adding Eq.(7) and Eq.(18), and using $M = IdA / 4\pi R$, gives:

$$E_Z = j\frac{\mu\omega dA \sin\theta(1 - jkR)\exp(jkR)}{4\pi R^2}\left[I_Y \cos\phi + I_X \sin\phi\right] \tag{19}$$

where $\mu = \mu_r\mu_o$. It is desirable that this composite beam be azimuth-referenced to either the X- or Y- axis by putting the bracketed term into either the form $Isin\zeta$ or $Icos\zeta$ respectively. The $Icos\zeta$-form is chosen to later avoid a negative sign. If we now write $I_X = I\sin\xi$, and $I_Y = I\cos\xi$, then E_z becomes:

$$E_Z = j\frac{\mu\omega dA \sin\theta(1 - jkR)\exp(jkR)}{4\pi R^2} I\cos(\xi - \phi) \tag{20}$$

The maximum positive field occurs along the line $\xi = \varphi$. In other words, we have only to multiply the two otherwise equal and in-phase loop currents by the sine and cosine of the azimuth angle at which the beam-maximum should be pointed[°]. The two-lobed E_z-field will cover the entire azimuth plane by steering the positive lobe through the ϕ-range of only $\pm 90°$. Because $cos(\xi)$ is positive over $-90° < \phi < 90°$, the trigonometric term in Eq.(20) is positive, and the bracket-term in Eq.(19) must be positive also. Therefore, it will be necessary to reverse the direction of current flow in HMD_X for $\phi < 0$.

Application to Class-D Power Amplifier. The Class-D power amplifier *(Caffey, 1965; Krauss et al.,1980)* offers efficiencies in excess of 90% by delivering a train of rectangular voltage pulses to a tuned circuit which here consists of an HMD-winding and a series-resonant capacitor. The peak value of the fundamental current is formulated by Fourier

[°] If the form $Isin\zeta$ had been chosen, we would have to remember the rule that ' $\xi = -\varphi$ '.

analysis in terms of the ratio of the pulse duration, τ, to the interval between the leading edges of successive pulses, T:

$$I_{Peak} = 2\frac{V_{CC}}{\pi R_{AC}}\left|\sin \eta\pi\right| \tag{21}$$

where: $\eta = \tau/T$, the duty cycle;
R_{AC} = Series AC resistance of the tuned load, Ohms;
and V_{CC} = Supply potential, volts.

The maximum current, $I_{Peak,Max} = 2V_{CC} / \pi R_{AC}$, occurs for $\eta = 0.5$. We agree to limit η to 0.5 because, for greater values, there will be increased heating of the active switching device due to its equivalent series output resistance and consequent decrease in efficiency.

There are two ways to change I_{peak} in accordance with the cosine-term of Eq.(20). One way is to change V_{CC}, and another is to vary the duty cycle, η. We chose this last method because it is readily done with digital circuitry.

When Eq.(21) is normalized by I_{Peak}, we can solve for η as a function of angle ϕ. We have, for HMD_X, $I_X = I \sin\xi$, and $\sin\xi = \sin\phi = \left|\sin\left(180\eta_X\right)\right|$, or

$$\eta_X = \phi / 180. \tag{22}$$

The duty cycle for HMD_Y is similarly found:

$$\eta_Y = Arc\sin\left[\cos\left(\phi\right)\right] / 180. \tag{23}$$

Suppose, for example, we wished to direct the positive lobe to $\phi = 125°$. This is outside the ϕ-range, so the negative lobe is directed by choosing $\phi = -55°$. We find that η_X = -0.306 and η_Y = 0.194. At an operating frequency of 1MHz we would need pulse widths of 306ns and 194ns respectively to point the negative lobe at 125°, and the negative sign for η_X advises that the direction of current flow in HMD_X must be reversed. This is readily done by delaying the HMD_X-pulse train by T/2.

Beam-steering was accomplished in 16 steps of 11.25° with the use of a programmable logic array, 'PLA', operated with a 16MHz clock.

Application to Class *E* Power Amplifier. The Class-E amplifier is another type of high-efficiency amplifier which also delivers a train of voltage pulses to a tuned circuit *(Sokal and Sokal, 1975; Raab, 1977, Kazimierczuk, 1983)*. We built and investigated this amplifier at the suggestion of our industrial partner who had experience with it. However, I_{Peak} cannot be linearly controlled by varying V_{CC}. The pulse shape is a function of the duty cycle *(Raab, 1978)* which would make the computation of the relative pulse widths

for Class-E steering exceptionally tedious and result in nonlinear control increments in the PLA. This possibility was not pursued further.

Beam-Steering in the Receiver. This is the best method but could not be used because of the lack of the integrated package. A single Class-D amplifier could be used with a fixed V_{CC} and $\eta = 0.5$. The two magnetic dipoles would be energized separately, and their individual currents would be digitized and stored as complex $(a + jb)$ words. The receiver output due to each dipole would also be digitized and stored as a complex word. Processing would begin by normalizing the X and Y signals by their respective antenna currents. Because the beam-steering angle reverts directly to ϕ, and ξ is not used, computer software can multiply the signals by the sine and cosine of ϕ and add them according to Eq.(19). This method would provide full 360° beam-steering at arbitrary angles under software control.

Range-to-Target

This section describes an algorithm for computing the range-to-target for a cw radar without requiring *a priori* knowledge of the electrical parameters of a homogeneous, isotropic medium between the radar and the target. The phase of the scattered signal is measured during a linear traverse along the borehole past the target. The furnished range is the minimum radial distance between the radar and some point on, or within, the target. The algorithm is developed below, the computer code is briefly described, and several examples are given.

Phase and Distance. The range algorithm is based on the measurement of phase. The phase of the E_Z-field from an HMD_x can be derived from Eq.(7) as

$$\phi_{E_Z} = \alpha R + (\pi / 2 - \xi) \tag{24}$$

where the factor 'ξ' is defined as $\xi = \text{Arctangent}\left(\frac{\alpha R}{1+\beta R}\right)$, and $0 \le \xi \le \pi / 2$. The range algorithm, as will be shown, substitutes trial numbers for the term $(\pi/2-\xi)$, so I will set that term to zero here, and solve for the distance over which the phase of E_Z is measured:

$$R = \phi / \alpha = \lambda\phi / 2\pi = \lambda\varphi / 360^\circ \tag{25}$$

where λ, the wavelength, is related to α by $\lambda = 2\pi/\alpha$.

The Traverse. Suppose the radar is translated in regular increments along its own axis and approaches, illuminates, and passes-by a discrete target as illustrated in Figure 9. As shown in Figure 10, the magnitude of the received signal will have a relative maximum near the point in the traverse where the range is a minimum, and the phase of the received signal will be a minimum near the same point. At each point the slant range is related to the measured round-trip phase by:

$$R_{p,i} = \left(\frac{\lambda}{360^\circ}\right)\left(\frac{\phi_i}{2}\right) = \frac{\lambda\phi_i}{720^\circ} \quad \text{meters,} \tag{26}$$

where:

$R_{p,i}$ = slant range from the midpoint of the antenna separation at the *i-th* traverse position, z_i; and

ϕ_i = round-trip phase, degrees.

The round-trip phase is divided by 2 because we wish to measure the one-way distance. $R_{p,i}$ will be called the *propagation* form of the slant range.

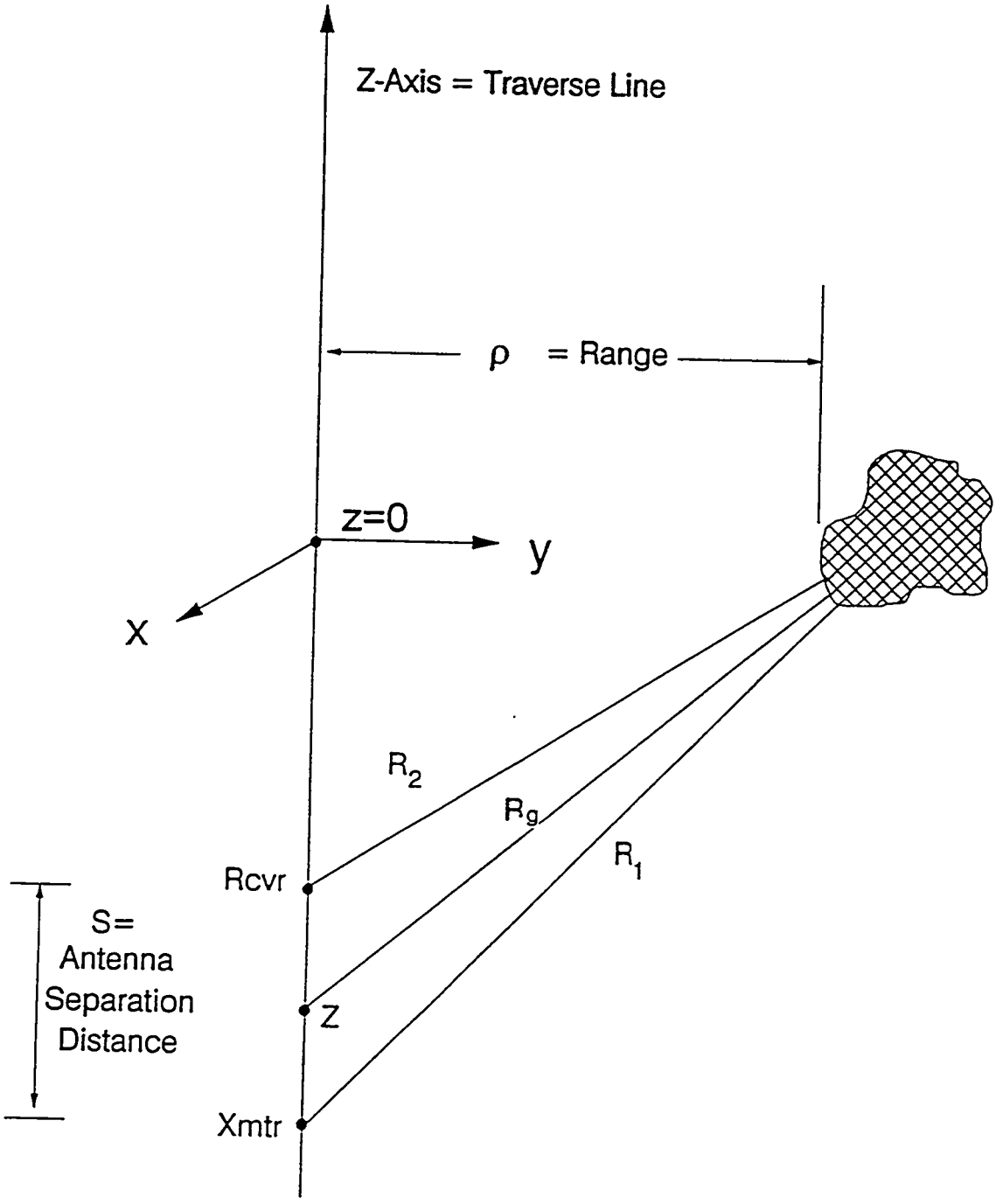

Figure 9
Measurement Geometry

twhc3_95

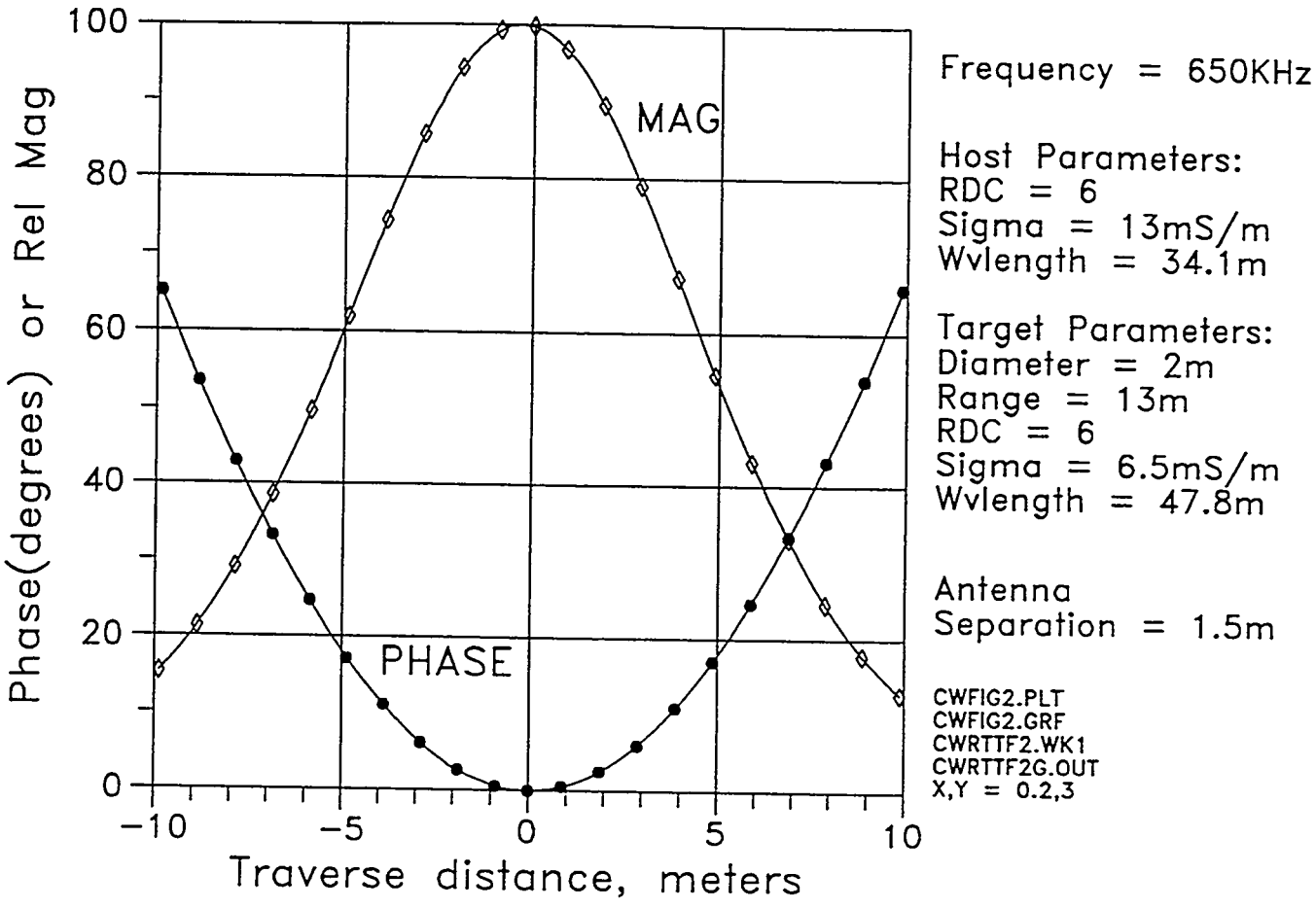

Figure 10
Traverse past a sphere in soil
Phase at center = 109 degrees

The minimum phase is denoted by ϕ_o, and the corresponding traverse distance is denoted by z_o. The minimum radial range is denoted ρ_o and given by a special form of Eq.(26):

$$\rho_o = \frac{\lambda \phi_o}{720} \qquad \text{meters.} \tag{27}$$

There are several problems with using Eq.(26) and Eq.(27): In practice, the phase is measured modulo 360°, and the number of 360°-increments which are included within the phase is unknown. Also, there is a phase shift which occurs upon reflection and which is included in the phase measurement. Additionally, the wavelength is unknown, and a further difficulty is that the two unknowns multiply each other!

The geometric form of the slant range from the midpoint of the antenna separation can also be set down from Figure 9:

$$R_{g,i} = \sqrt{\rho_o^2 + z_i^2} \quad . \tag{28}$$

The two forms for the slant range, propagation and geometric, are the basis of the algorithm.

Approximation Error. The geometric slant range is an approximation to one-half the round trip range from the transmitter to the receiver, and the error must be examined before proceeding. Denoting the slant distances from the transmitter and receiver to the target by $R_{1,i}$ and $R_{2,i}$ respectively, the round-trip path length, R_{rt}, is the sum of $R_{1,i}$ and $R_{2,i}$. What is the error in using $R_{g,i} = R_{rt,i} / 2$? $R_{1,i}$ and $R_{2,i}$ can be written in terms of $R_{g,i}$ as follows:

$$R_{1,i} = R_{g,i} \sqrt{1 + \frac{s^2 + 4sz_i}{4R_{g,i}^2}} \quad , \tag{29}$$

$$R_{2,i} = R_{g,i} \sqrt{1 + \frac{s^2 - 4sz_i}{4R_{g,i}^2}} \quad , \tag{30}$$

and,

$$\frac{\left(R_{rt,i} / 2\right)}{R_{g,i}} = \frac{\sqrt{1 + \frac{\eta^2 + 4\eta\Gamma_i}{4 + 4\Gamma_i^2}} + \sqrt{1 + \frac{\eta^2 - 4\eta\Gamma_i}{4 + 4\Gamma_i^2}}}{2} \quad , \tag{31}$$

where: $\eta = s / \rho_0$ is the normalized separation distance, and
$\Gamma_i = |z_i / \rho_o|$ is the normalized traverse distance.

The error in using $R_{g,i}$ for the slant distance is plotted in Figure 11, and two conclusions are: (1) The error is greatest when the traverse distance is zero, and (2) The separation distance should be made as small as possible consistent with crosstalk constraints.

Hyperbolic Response. The phase response in Figure 10 appears that it might be hyperbolic, and this is confirmed by equating $R_{p,i} = R_{g,i}$ and using the definition of ρ_o:

$$\frac{\phi_i^2}{\phi_o^2} - \frac{z_i^2}{\rho_o^2} = 1 \,. \tag{32}$$

This is the standard form of an hyperbola which is centered at $\phi_o = 0$.

Difference Function. The key idea in the algorithm consists of taking the magnitude of the difference between $R_{g,i}^2$ and $R_{p,i}^2$, namely

$$\text{Difference Function} = \left| \left(z_i^2 + \left[\phi_o \lambda_j \,/\, 720 \right]^2 \right) - (\phi_i \lambda_j \,/\, 720)^2 \right|, \quad \text{i} = 0,\, 1,\ldots \tag{33}$$

where the λ_j are trial values of wavelength, $j = 1,2,\ldots j_{\max}$. At $i = 0$, $z_i = 0$, $\phi_i = \phi_o$, and the DF is zero.

The ϕ_i are now replaced by a new phase variable, Φ_i, so that adjustments can be introduced:

$$\Phi_i = \phi_i + \psi_k + 360N \tag{34}$$

where:

N = the *phase adjustment index* which allows trial restorations of the 360°-increments which may have been removed; $N = 0,1,\ldots N_{\max}$;

and

ψ_k = trial values of the ξ-factor and reflection phase combined; $k = 1,2\ldots k_{\max}$.

With the use of Φ_i, the DF becomes

$$\text{DF} = \left| (720 z_i)^2 + \lambda_j^2 \left((\phi_0 - \phi_i)(2\psi_k + \phi_0 + \phi_i + 720N) \right) \right|. \tag{35}$$

The Φ_i, like the ϕ_i, must always be ≥ 0 to prohibit the computation of a negative range. The sum of ϕ_i and ψ_k may cover the range from 0°-to-360° for each choice of N. Ac-

RANGEROR.PLT
RANGEROR.GRF
RANGEROR.WK1
X,Y = −0.5,3

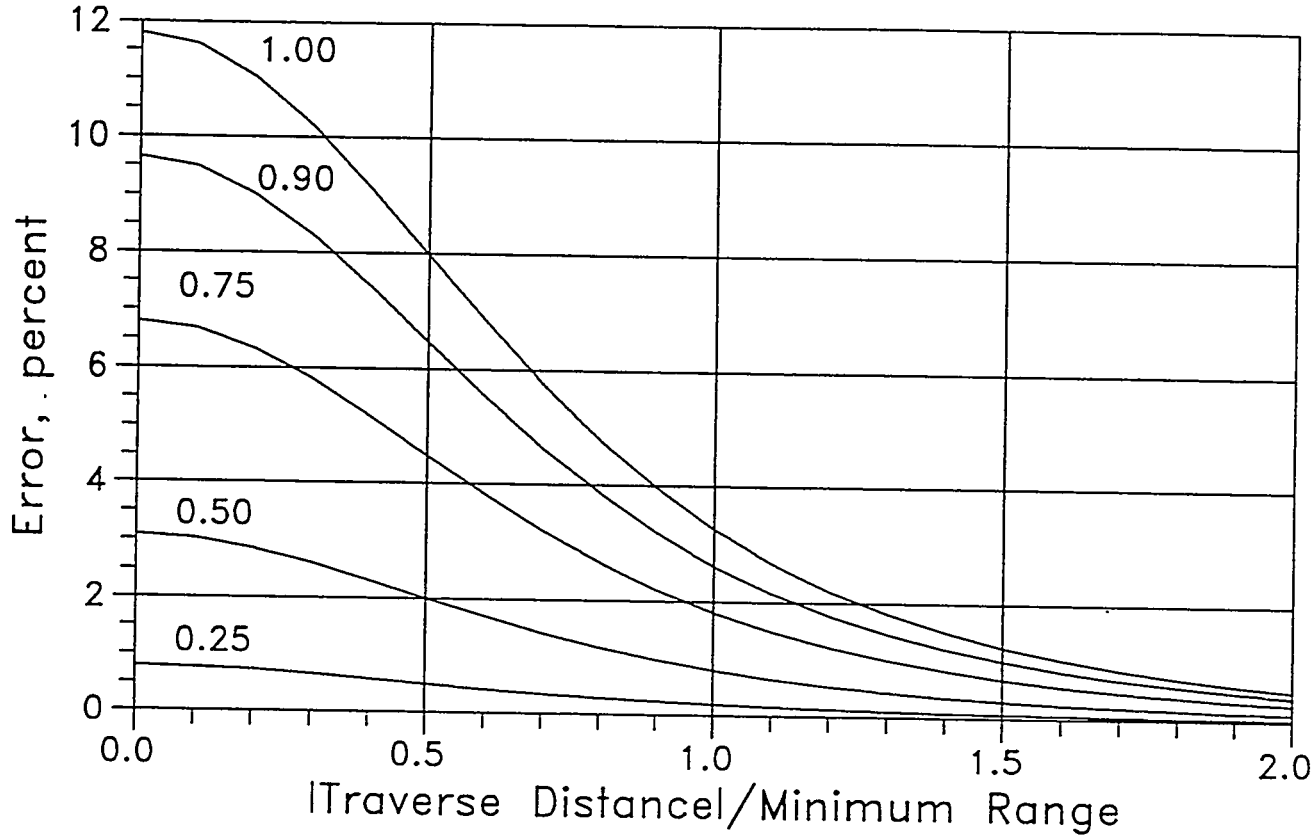

Figure 11
Error in midpoint approximation
with Separation/(Minimum Range)
as a parameter

cordingly, $-\phi_i \le \psi_k \le (360 - \phi_i)$; that is, negative values of ψ_k are permitted. This interval is searched with a uniform increment $\Delta\psi$ which is a free choice.

If the mean difference function over the (ϕ_i, z_i) is minimized over the indicial set $\{j,k\}$ for each N, including the point $\phi_i = \phi_0$, the global minimum should provide the range which is most consistent with the data. This process is called the *difference method* after the concept of Eq.(33).

A second way to obtain the range is based on the observation that Eq.(33) can be set to zero and solved directly for ψ_k for each choice of ϕ_i, λ_j, and N:

$$\psi_k = \frac{(720 z_i)^2}{(\phi_i - \phi_0)\lambda_j^2} - (\phi_i + \phi_0 + 720N), \qquad i \neq 0. \tag{36}$$

subject to the constraint that $-\phi_i \le \psi_k \le (360 - \phi_i)$. The ψ_k obtained for each (i,j,N) are averaged over the $(i-1)$ data points to obtain a trial value ψ_k, and the λ_j and ψ_k are used as before to obtain a minimum of the mean difference function. This second method is called the *direct solution* method because trial values of ψ_k are directly obtained.

Precision Effects. The range-to-target algorithm is a numerical solution process and must be constrained to avoid instability, unwarranted precision, and results that are physically impossible. Accordingly, to minimize the effect of round-off errors, the (z_i, ϕ_i)-data are read-in as double-precision numbers, and the computations are performed in double precision.

One problem arises from the limited precision of the phase measurement itself. The several values of ϕ_i in the vicinity of the apex of the hyperbola usually have the same value. If the number of such values is odd, the middle value is chosen as ϕ_o; if the number is even, the mean value of the two z_i in the center is inserted as z_o and a corresponding ϕ_o is likewise inserted. The z_i are subsequently recalculated so that only $z_o = 0$.

Wavelength Estimates. Because the range solution requires both phase and wavelength, and only phase data are supplied, it is necessary to make an initial guess for the wavelength. Because the wavelength is computed from the electrical parameters, it is more direct to use estimates of the lower and upper limits of each of the electrical parameters. The relative magnetic permeability 'μ_r' is taken as unity, and two values for both the relative dielectric constant and the conductivity must be supplied. The wavelength in the media is given by

$$\lambda = 2\pi / \alpha \ , \tag{37}$$

where α is the real part of the media propagation constant 'k' given after Eq.(2). The smaller wavelength limit λ_{min} is computed using $(\varepsilon_{r,max}, \sigma_{max})$, and the greater wavelength limit λ_{max} is computed with $(\varepsilon_{r,min}, \sigma_{min})$. The wavelength-interval from λ_{min} to λ_{max} is searched with a uniform increment $\Delta\lambda$ which is a free choice.

Range Constraints. A minimum and maximum range exists for each choice of N. The radial distance, in terms of the search variables, is written as

$$\rho_{i,j,k,N} = \frac{\lambda_j \Phi_i}{720} = \frac{\lambda_j (\phi_i + \psi_k + 360N)}{720}, \qquad (38)$$

which gives: $\rho_{min,N} = N\lambda_{min}/2$, and $\rho_{max,N} = (N+1)\lambda_{max}/2$. (39a,b)

These range-extremes permit overlapping range-intervals for successive choices of N; that is, $\rho_{min,N+1} < \rho_{max,N}$ as shown in this table for the first few values of N:

..N..	.....ρ_{min}.....	.....ρ_{max}.....	..... $\rho_{max} - \rho_{min}$ .....
0	0	$1\lambda_{max}/2$	$\lambda_{max}/2$
1	$1\lambda_{min}/2$	$2\lambda_{max}/2$	$(2\lambda_{max} - \lambda_{min})/2$
2	$2\lambda_{min}/2$	$3\lambda_{max}/2$	$(3\lambda_{max} - 2\lambda_{min}/2$
3	$3\lambda_{min}/2$	$4\lambda_{max}/2$	$(4\lambda_{max} - 3\lambda_{min})/2$

Computer Code. The present phase-search code, *PHSRCH*, consists of over 600 non-commented source statements written in Microsoft® FORTRAN Version 5.1. The input data are extensively checked, and intermediate results are continually checked to ensure that they are within the constraints imposed by wavelength, ψ-limits, and range.

Psi-Break. The code proceeds by finding a minimum value of the *DF* for increasing values of N. Determining which of the minimum *DF*s corresponded to the correct solution was elusive. The explanation lies in Eq.(38) where, as N increases, λ_j decreases with possible increases in ψ_k permitted by ρ_{max}. The range constraint eventually breaks the monotonic increase of Psi-Adjust values as shown by this partial output listing:

N-Phs	Wave Length meters	Minimum Mean Dif Ftn	Range meters	'ψ_k' Psi-Adjust degrees
0	10.2	.220E+00	3.16	-45.3
1	10.1	.143E-02	9.38	40.3
2	8.1	.151E-03	12.15	91.3
3	7.1	.116E-03	14.01	72.3
4	6.6	.101E-03	15.11	-60.3

The ψ_k in the right-hand column increase with N, but, beginning with $N = 3$, the ψ_k decrease. The value of N at which the decrease begins is termed the "Psi-break", and an acceptable answer has not been observed either at a Psi-break or afterwards. The solutions for $N = 3,4$ are discarded, and the difference function for $N = 2$ is seen to be almost 10-times smaller than that for $N = 1$. This identifies 12.15m as the range.

Examples. Several examples are given below which demonstrate the usefulness of the algorithm in air and in three increasingly conductive soils. Except for the last example, the transmitter is a magnetic dipole aligned along the positive X-axis, and the receiver is an electric dipole aligned along the positive Z-axis and 1.5m above the transmitter. A 3D-sphercial target code is used which was developed from the derivation of Debye potentials given by March*(1929, 1953)*. Results are given only for the direct solution method which is more satisfactory because it is not necessary to use $\Delta\psi$. Accuracy is improved if only those data points are used which occur as the radar approaches the target because of the slight asymmetry introduced by the antenna separation distance.

Air Example. The target is a 1m OD sphere, with $\varepsilon_r = 1$ and $\sigma = 1.0S/m$, centered 25m from the traverse line in air. At 100MHz the minimum round-trip phase to the target surface is 2942°. The traverse extends ±3.25m in 0.1m intervals and provides extreme phases of 84.9° centered on $\phi_0 = 34.5°$. Using just the 3 extreme phase values on the approaching side together with ϕ_0, 4 points in all, the estimated range is 25.26m ± 0.03m which is within the target limits of 24.5m -to - 25.5m.

Moderate Soil Example. The Boulder Creek granite formation near Raymond, Colorado, has been extensively measured *in situ* at frequencies up to 25MHz *[Grubb et al. 1976]*. At 7.6MHz the parameters are $\varepsilon_r = 9$ and $\sigma = 1.6mS/m$ which provide a wavelength of 12.88m. A 1m OD spherical target is centered 2 wavelengths, or 25.76m, away. The target RDC is the same as the host, but two conductivities are used: Four times the host value and one-fourth the host value. The traverses extend ±7.65m in 0.15m intervals and provide extreme phases of 328° and 127° centered on $\phi_0 = 266.4°$ and 64.8° respectively. The two range estimates, using 4 points, are identical: 25.80m ± 0.05m, which is within the permitted limits of 25.26m - to -26.26m.

Conductive Soil Example. This is a set of 3 examples to show the effect of increasing frequency upon the determination of range with a 2m OD target centered at 13m. The host media has a conductivity of 13mS/m, and the target conductivity is 6.5mS/m. The RDC is 6 for both host and target. Frequencies of 0.65MHz, 2.6MHz, and 10.4MHz are used, and Figure 10 is a plot of the 650kHz data. The three phase values for each frequency are within 62.4° - 64.4° of ϕ_o. The results are:

Frequency, MHz	Range, meters	N
0.65	13.95 ± 0.10	0
2.6	13.23 ± 0.05	1
10.4	12.13 ± 0.03	2

All three range estimates are within the target, but move from the rear of the target toward the front as frequency is increased. However, operating at 2.5MHz and 10.4MHz requires power increases of 11dB and 47dB respectively compared to 650KHz.

A Blind Example. L. C. Bartel, Dept. 6116, submitted 5KHz data, prepared for another use and illustrated in Figure 12, as a "blind test" for the algorithm. The data are simulated for a surface traverse using vertical magnetic dipoles separated by 10m with a traverse increment of 10m. A good hyperbola is obtained if the center point and the 2nd and 3rd point on each side are retained. Using the center point and 2nd and 3rd point on the approaching leg, 3 points in all, the furnished range is 27.9m $\pm$ 0.3m. The uncertainty quoted here is too small because, from Figure 11, a 2% error, about 0.56m, occurs in the midpoint approximation. The combined uncertainty is about $\pm$0.7m which still places the range within the target limits of 20m-to-30m.

Crosswell Example. If the transmitter and receiver are horizontally separated, and one is traversed past the other, the hyperbolic phase response is still obtained. In this example the antennas are placed 31.4m apart in the Boulder Creek media at 10.2MHz for which the conductivity is 1.75mS/m and the RDC is about 8.2. Because the path is now one-way, the algorithm is modified by replacing the factor of 720 degrees by 360 degrees in Eq.(35). There is no reflection phase, so the ψ_k are set to zero. The computed range in this case is 31.4m $\pm$ 0.2m which is in good agreement with the separation distance.

Figure 12

Profile for 10 m Separation

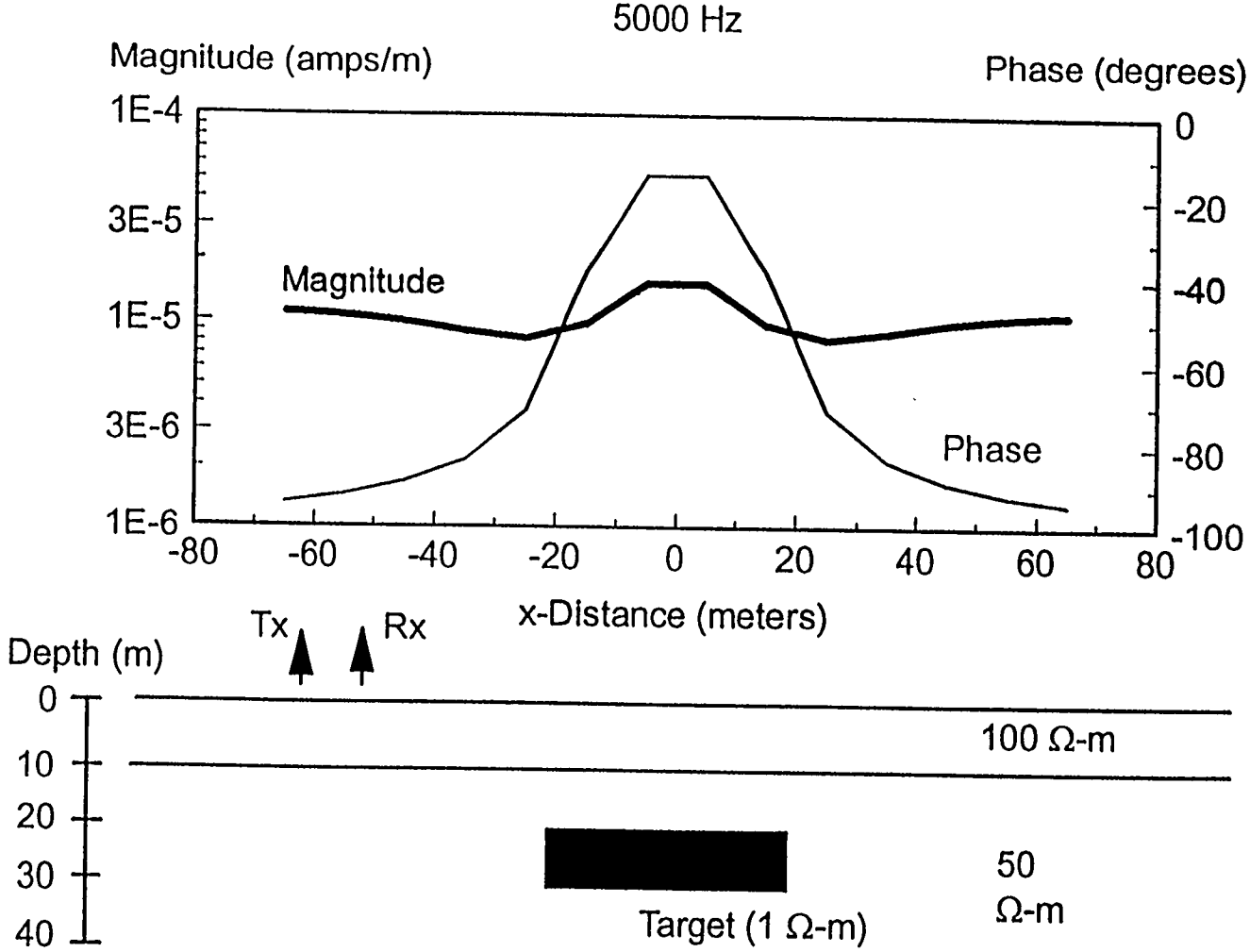

Apparatus

An overall layout of the package, 366cm long by 9.3cm OD, is shown in Figure 13. Two analog fiber-optic links, 30m long, one from the transmitter to observe the HMD-current, and one from the receiver to provide the observed signal, were used for communication from the package to the surface. There was no provision for communication from the surface down to the package.

Receiver Details. The receiver was partly described in the earlier section on crosstalk, and was built within the upper-most electrode to prevent the receiver electronics from contaminating the incident electric field. The battery pack consisted of four 3.6V Lithium cells, and was also enclosed in the upper electrode. The schematic, Figure 14, shows two stages of signal amplification which drive a biased amplifier for the fiber-optic transmitter. The high-frequency, -3dB corner frequency of the input is about 1.25MHz, and the total thermal noise density referred to the input is about 3.1nVrms per root-Hertz. The fiber-optic transmitter was designed together with the fiber-optic receiver, Figure 15, to provide a gain of about unity over the fiber-optic link or 'FOL'. The design gain of the receiver through the FOL is about 3800x, and the measured gain was 4050x. There are at least two effects which may make the signal-gain, the amplification of the voltage difference across the gap, less than the design gain.

In order to estimate the signal gain of the receiver, we need to estimate the source impedance of the equivalent voltage generator which supplies the potential difference between the electrodes to the amplifier input. This source impedance is in series with the 330pF capacitor and 385Ω resistor across the amplifier input. This series-shunt combination makes V_{in} less than the open-circuit voltage at the antenna terminals according to

$$\frac{V_{in}}{V_{open-circuit}} = \frac{Z_{in}}{Z_{source} + Z_{in}} \quad . \tag{38}$$

Equation (38) is the *voltage-divider ratio* or *VDR*, and Z_{in} is the impedance of the parallel combination of the input capacitor and resistor, namely $Z_{in} = \{235 - j188\}\ \Omega$ at 1MHz.

The impedance of the gap itself is in parallel with Z_{in} and may possibly reduce the *VDR*. The impedance of the gap between the electrodes at 1MHz, including the Lexan tubing and the fiberglass support tube, was measured as a 909KΩ resistance in parallel with a 23.5pF capacitor with a reactance of 6770Ω. This combination was so large that neither Z_{in} nor the VDR were affected.

As shown in Figure 7, each receiver electrode is in contact with a cylindrical Lexan™ radome which is centered in an air gap within a PVC casing. The air cap, casing, and host media form a sequence of cylindrical shells in shunt with the radome. The precise effect of the sequence is hard to determine, but it seems reasonable to estimate that the impedance

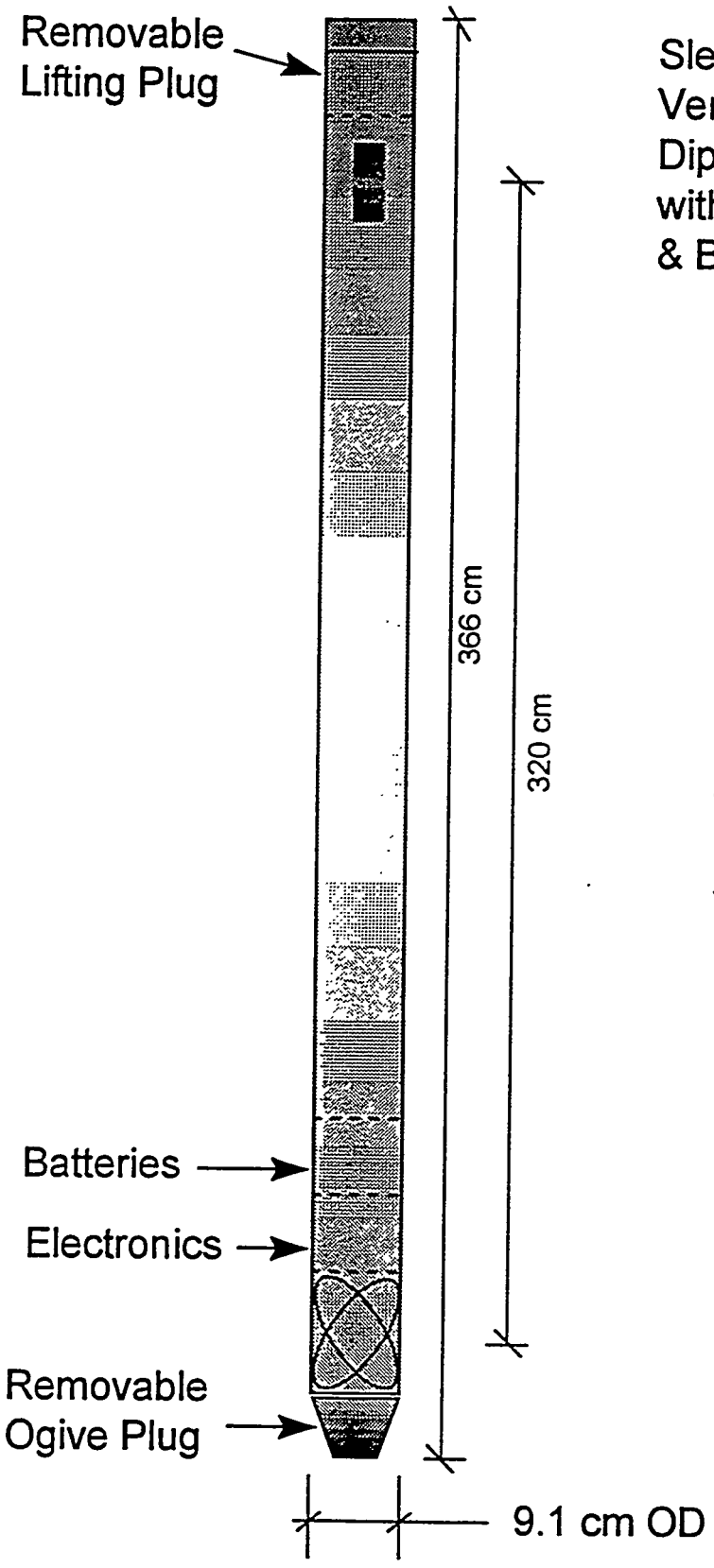

Sleeve Type
Vertical Electric
Dipole Antenna
with Electronics
& Batteries Inside

Figure 13
Layout of
Borehole Radar

Transverse
Scale is 2 times
Vertical Scale

Orthogonal
Horizontal
Magnetic Dipoles

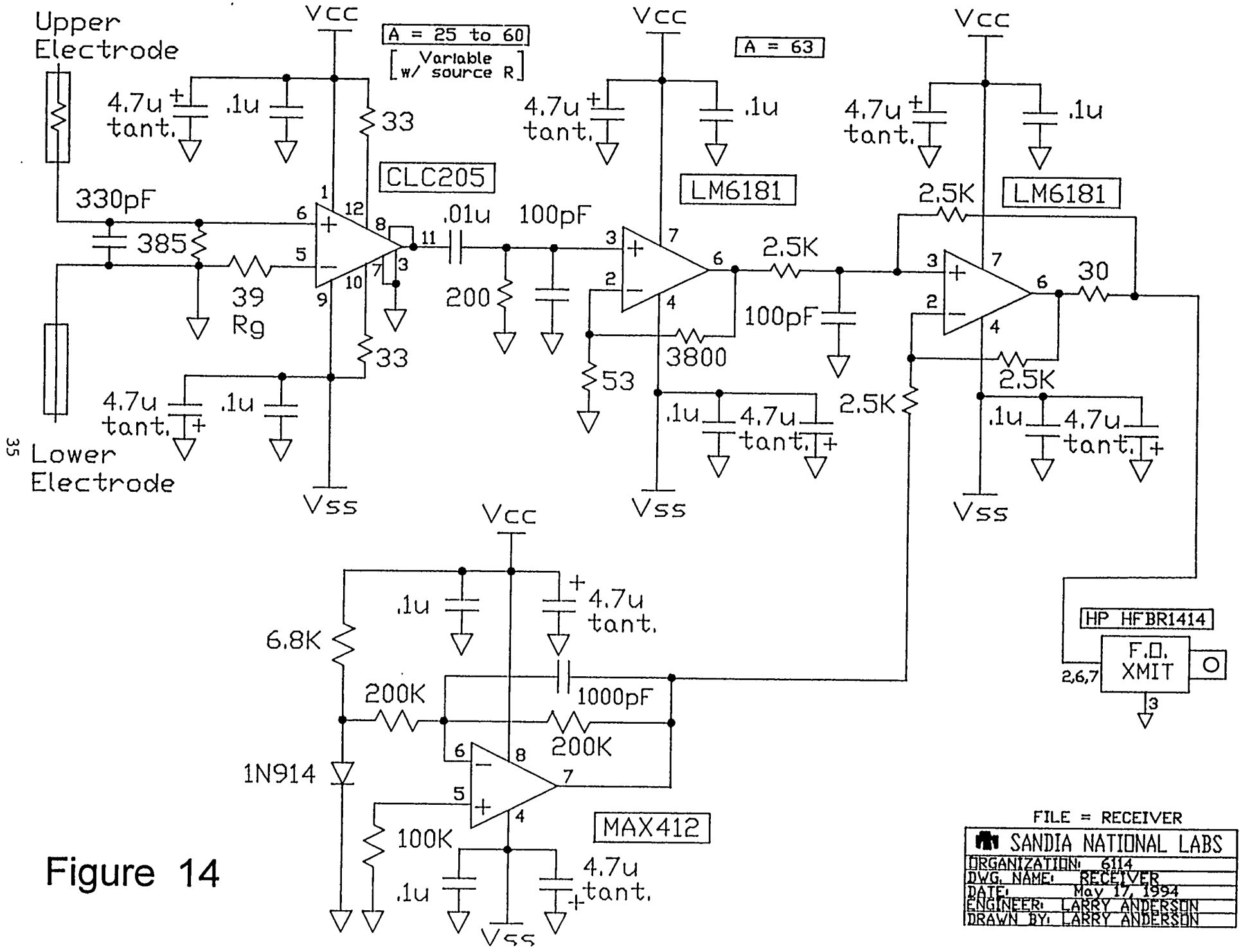

Figure 14

FILE = RECEIVER

SANDIA NATIONAL LABS	
ORGANIZATION:	6114
DWG. NAME:	RECEIVER
DATE:	May 17, 1994
ENGINEER:	LARRY ANDERSON
DRAWN BY:	LARRY ANDERSON

FIBER OPTIC RECEIVER

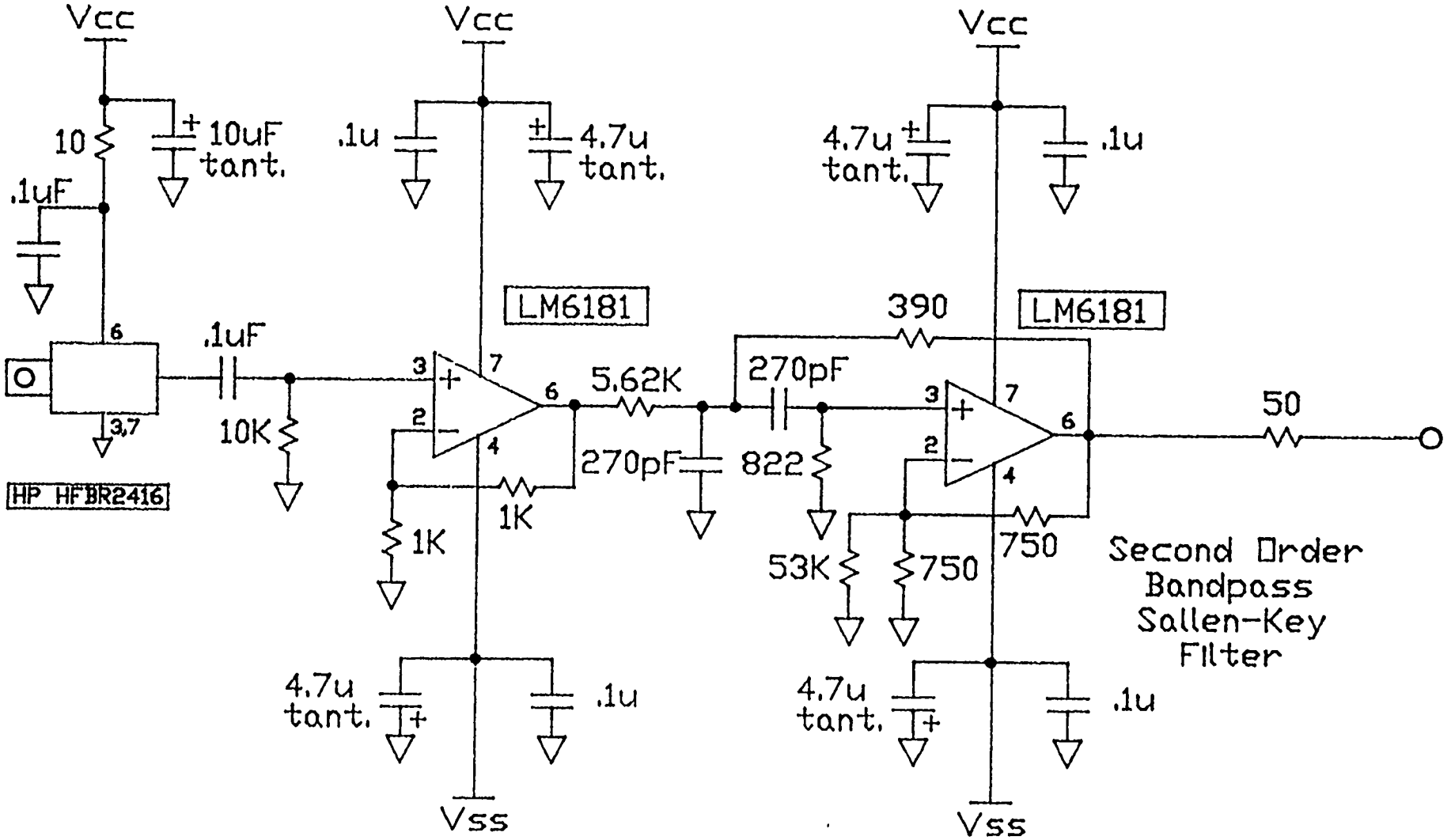

Buffer Amplifier

A = 2

Filter and Cable Driver

Fc = 1MHz

Q = 10

A = 2

NOTE: Vcc = +5V

Vss = -5V

FILE = FO_box

SANDIA NATIONAL LABS	
ORGANIZATION:	6114
DWG. NAME:	F.O. Receiver
DATE:	May 17, 1994
ENGINEER:	LARRY ANDERSON
DRAWN BY:	LARRY ANDERSON

Figure 15

in series with the input does not exceed the wave impedance of the radome *(Schelkunoff and Friis, 1951):*

$$Z_{source} = Z_{wave} = Z_o \sqrt{\left(\frac{\mu_r}{\varepsilon_r}\right) \bullet \left(\frac{1}{1 - jg}\right)} \qquad (39)$$

where Z_o is the wave impedance of free-space, about 120π Ohms. In almost all earth media, it is safe to regard $\mu_r \approx 1$. If the loss tangent 'g' is >> 1, then the VDR is very nearly Z_{in}, but for small values of 'g' the effect of Z_{source} may be deleterious.

At 1MHz, $Z_{source} = \{15.5 + j15.4\}\Omega$ for Lexan, and $VDR = 0.99 \angle -4.1°$ which is very close to unity as desired. This assumption of simply using radome parameters to compute the *VDR* may be challenged with the argument that, at 1MHz, the PVC casing, the air gap, and the Lexan radome are all virtually transparent to the propagation of an E_Z-field approaching the antenna from within the media. Accordingly, the VDR was computed for a wide range of media parameters. The VDR-magnitude is reduced by less than 9%, and its phase is affected by less than 11.5 degrees, whenever the conductivity is ≥ 2mS/m over the range of relative dielectric constants from 3-thru-81. This was considered acceptable because the conductivity in the vicinity of the test wells had been measured in the range from 8-to-15 mS/m, and the VDR-magnitude is reduced by less than 2% at 8 mS/m.

The Z_{wave} for the HMD_X can be formulated by writing $H_\phi = -H_X \sin\phi + H_Y \cos\phi$, and dividing H_ϕ into E_Z. The resulting expression is a function of (R, θ, ϕ), but this level of complexity is not useful because there is no likelihood that the return-wave emanates from an HMD_X! The Z_{wave} given by Eq.(39) is used because it is the simplest form, and because the receiving antenna dimensions are so small compared to the wavelength of the incident field that it is reasonable to assume, for practical purposes, that the incident wave is plane whatever its actual sources(s).

The bandwidth of the receiver is set by the filter in the FOL receiver to about 200kHz centered on 1MHz. Further filtering was selected as needed in the spectrum analyzer and phase meter shown in the block diagram, Figure 16.

Transmitter Details. The transmitter was partly described in the earlier section on crosstalk, and was installed at the far end of the package from the receiver to maximize separation.

Both magnetic dipoles were wound on a 7.46cm OD cylindrical Lexan tube. Each winding consisted of 29 turns of #34 copper wire. The wire for each winding was fed through holes which were radially drilled through the sides of the form and equally-spaced around a 90° arc on opposite sides of the form on both top and bottom. Although the area-per-turn decreased slowly on either side of the middle turn, the total area was $0.20m^2$ for each winding. The holes for one winding were offset axially 0.5cm and 90° from the other

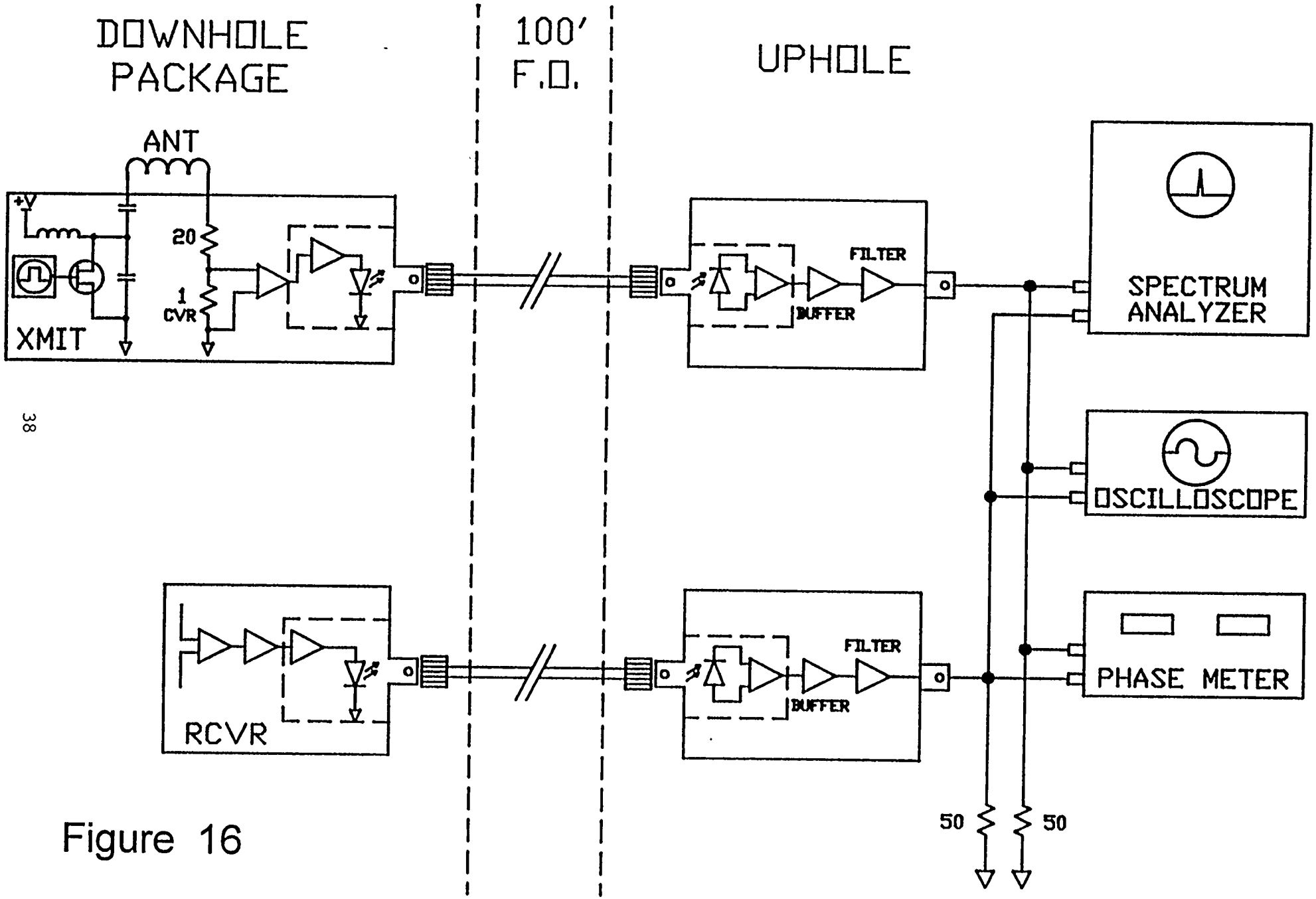
DOWNHOLE
PACKAGE
100'
F.O.
UPHOLE
ANT
+V
20
1
CVR
XMIT
FILTER
BUFFER
SPECTRUM
ANALYZER
OSCILLOSCOPE
RCVR
FILTER
BUFFER
PHASE METER
50
50

Figure 16

winding to provide a compact design. Each winding had a Q-factor of about 40.6, an inductance of 53.2 μH, and a resistance of 8.2Ω. Eleven ohms was added in series to each winding to reduce the peak current to 0.332 amperes. The power dissipated in each loop was about 0.45 Watts, and about 0.60 Watts was dissipated in each series resistance. The total power drawn from the batteries was about 1.1 Watts for a supply-to-signal conversion efficiency of 96%.

The schematic, Figure 17, shows two transformer-less Class-D power amplifiers which were made possible by using complimentary semiconductor devices. A single fiber-optic transmitter was used to send the current waveform from one winding to the surface. The Programmable Logic Device, or PLD, was clocked from a 16MHz crystal oscillator, 16-times the operating frequency of 1MHz, because the 11.25°-steering increment was one-sixteenth of 180°. Two battery packs were used. One pack consisted of six 3.6V Lithium cells, with two sets of three cells first connected in parallel and then connected in series. This pack provided -7.2 volts to the fiber-optic driver and its bias stage. The transmitter electronics and first battery pack were located just above the windings within the winding form so that the windings were each driven from one end. The second pack, consisting of ten enhanced-capacity D-cells, provided 14.4 volts to separate regulators which supplied 5V and 10V. This pack was placed above the transmitter within the separator tube. All of the battery packs here, and in the receiver, had lifetimes in excess of 12 hours.

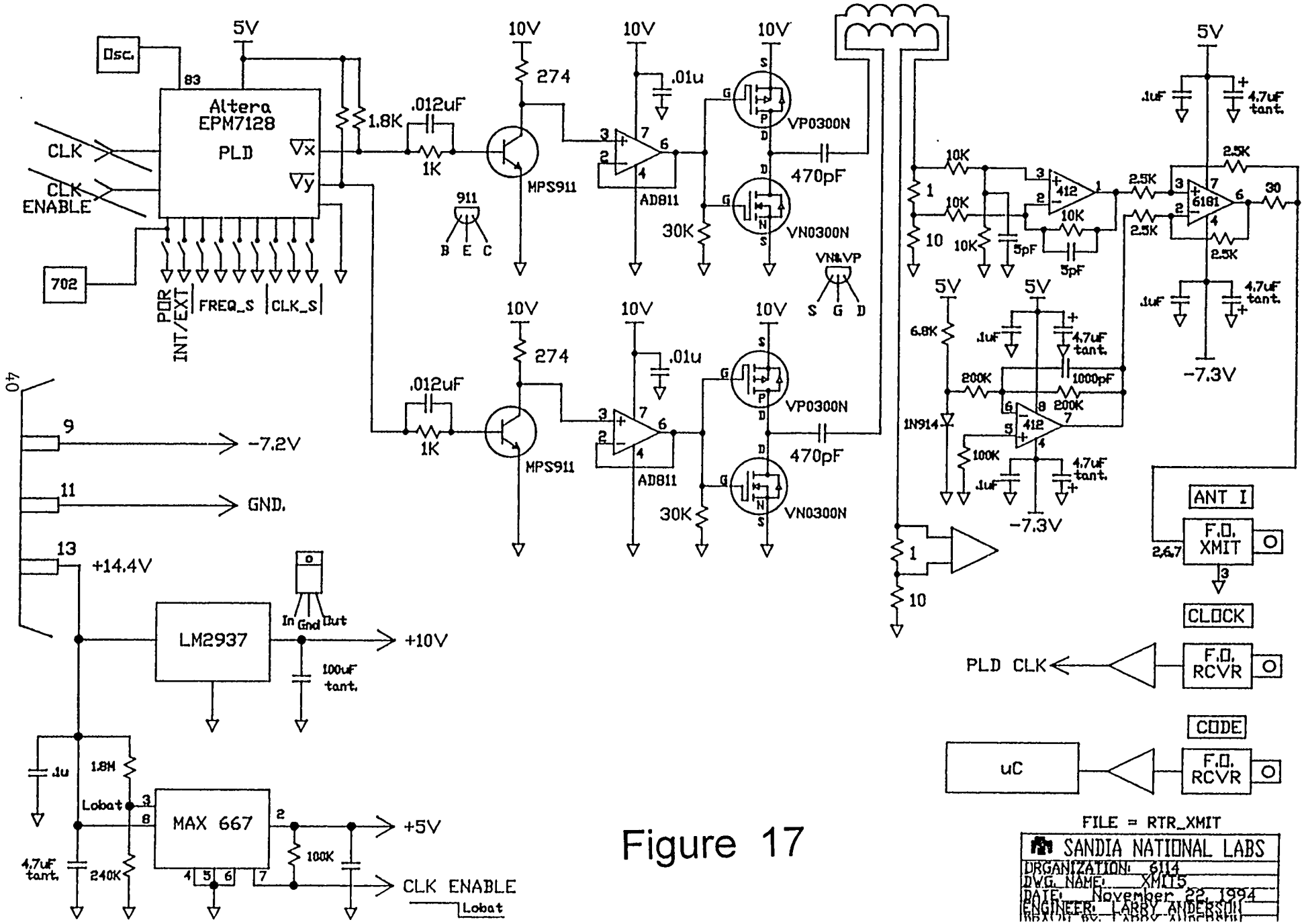

Figure 17

FILE = RTR_XMIT

SANDIA NATIONAL LABS
ORGANIZATION: 6114
DVG. NAME: XMIT5
DATE: November 22, 1994
ENGINEER: LARRY ANDERSON
DRAWN BY: LARRY ANDERSON

Field Measurements

Measurements were made just north of the Mixed Waste Landfill in Area III at Sandia/Albuquerque to demonstrate the existence of the bi-lobe beam pattern in the azimuth plane, and that targets could be detected with electronic beam-steering.

The layout of the boreholes is shown in Figure 18 where Well 'HW2' is 25m north of the landfill. The site is a deep fluvial bed from the Manzano Mountains several miles to the east. HW2 has a surface casing of steel pipe, 6.1m deep and 0.36m OD, which surrounds a 0.14m OD PVC casing which extends to a depth of 131m. The other two boreholes have the same PVC casing to a depth of 23m, but the surface casings are only 0.23m OD by about 0.91m deep. Operational depth to the package top was limited to about 12m because we did not have the magnetic compass which was to be part of the integrated package. Instead, we had to rely on sighting an index-mark on the top of the package with a sunlit mirror.

Beam Magnitude in the Azimuth Plane. The receiver was lowered to a depth of 9.7m in PVC-1, and the transmitter was lowered to 10.8m in PVC-2. A 360° protractor was transferred in 5° increments to the rim of the transmitter-well PVC casing. An index mark on the top of the transmitter was used to indicate the azimuth of the axis of the bi-lobe pattern by comparison to the protractor. Only the HMD_X was used, and rotational adjustments were made by hand. The comparison with the predicted pattern is shown in Figure 19 where the diameter of the dots is used to indicate an uncertainty of ±3° in azimuth and about 1cm in elevation. The agreement is very good, although there is some noticeable 'bounce' in the two nulls at small signal-to-noise ratios.

Electronic Azimuth Scan of Two Targets. The complete package, in the free-running, electronic beam-steering mode, was lowered to 12.2m in PVC-2 and the magnetic azimuth of HMD_Y was noted. The received signal is plotted against azimuth angle in Figure 20 where the 180° scan is plotted twice in succession to provide a 360° scan. The minimum phase occurs at the angular position of HW2, and the maximum phase occurs at PVC-1 as shown in the table of Figure 18. The magnitude plot of Figure 20 is not informative.

Conclusions

A radar system, as the name implies, must be able to detect a target and provide the spherical range to the target. These attributes have been demonstrated, but the azimuth-bearing to the target is ambiguous by ±180° because of the bi-lobed beam. We were not successful in reducing the beam to a single-lobe without making the lobe very broad in azimuth and introducing crosstalk. The range algorithm should be tested in more complex lithography and targets representative of oil, gas, and geothermal reservoirs with the use of 3D-modelling codes which are now available *[Newman and Alumbaugh, 1996]*. The operation of the elementary system described in this report shows that the concept of a continuous-wave borehole radar is robust, and should be pursued further.

Layout of Wells

Compass Bearings (°)

From PVC-2 to PVC-1:	279.6
From PVC-2 to HW2:	221.3
From PVC-1 to PVC-2:	199.6
From PVC-2 to HW2:	203.8
From HW2 to PVC-1:	23.8
From HW2 to PVC-2:	41.3

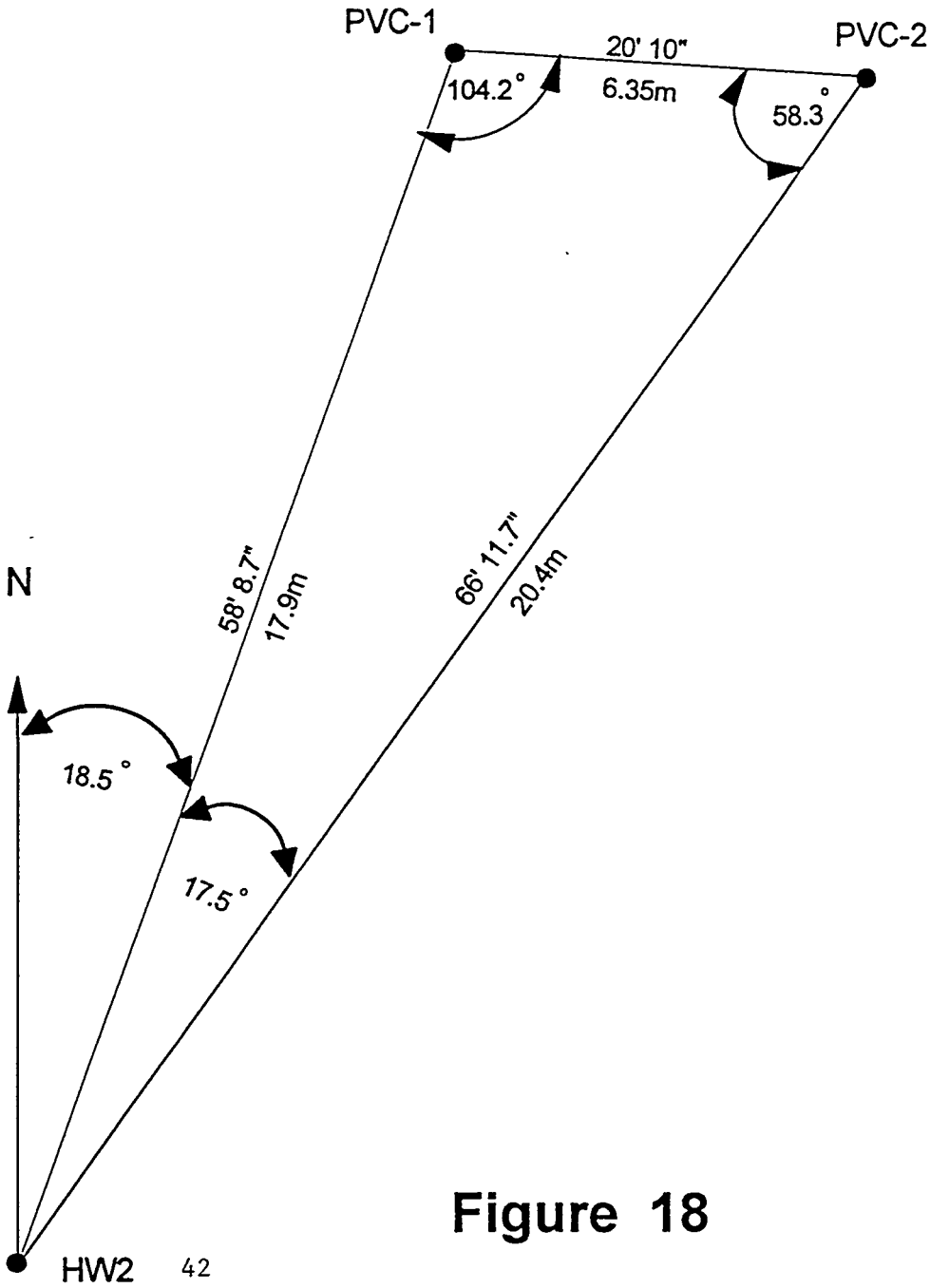

Figure 18

HT12P.DAT
HT12Q.DAT
HT12P.DCF

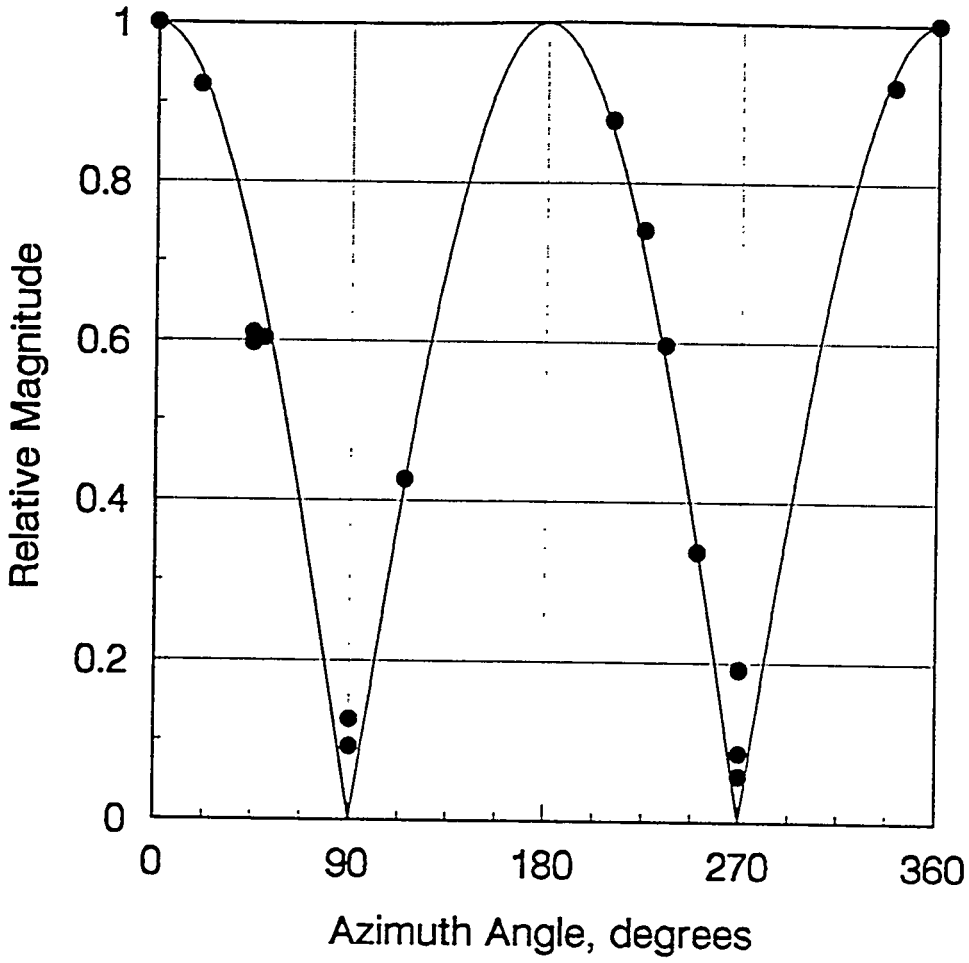

Figure 19
Beam Magnitude in the Azimuth Plane

'ST14A.WK1
'14XGT.DAT
'14XGT.DCF

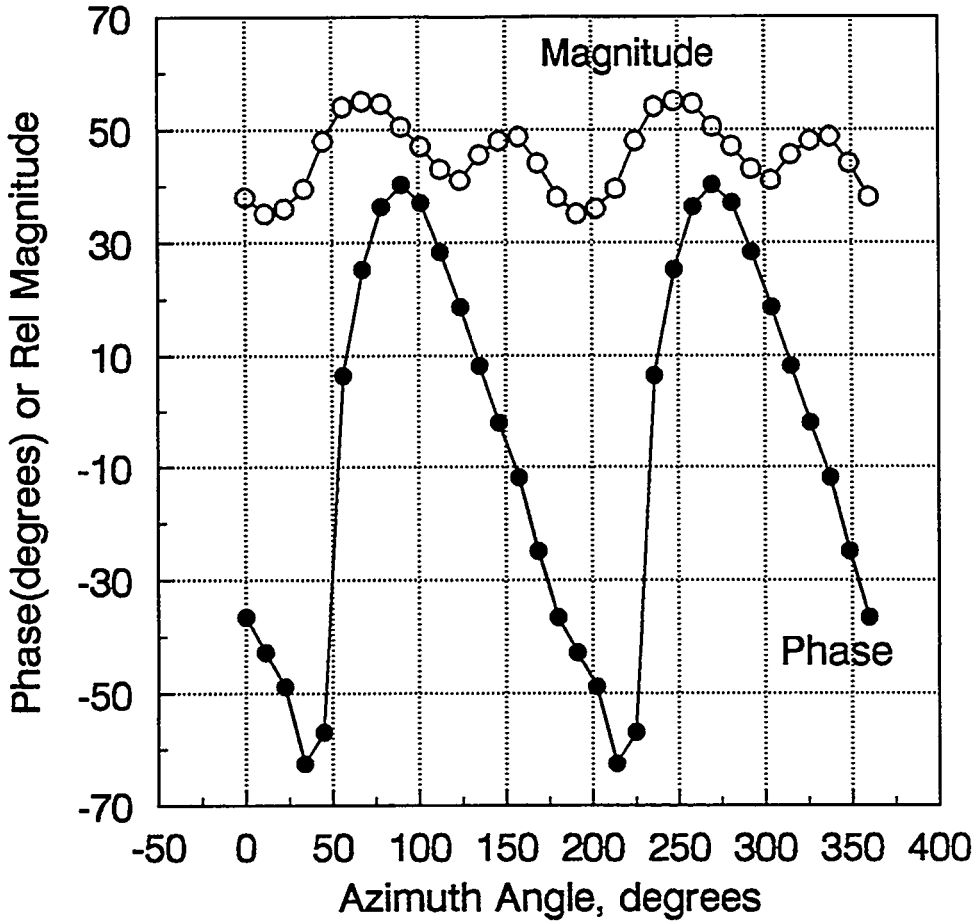

Figure 20
Electronic Azimuth Scan of Two Targets
Target 1 = 0.36m x 6.1m steel casing at 20.4m
Located at 41 and 221 degrees
Target 2 = 0.14m x 23m dielectric tube at 6.35m
Located at 100 and 280 degrees

References

in alphabetical order by the last name of the first author

T. W. H. Caffey, 1965, *The Voltage-Switching Class-D Amplifier*, Sandia National Laboratories Report SCDR65-338.

R. De Vore and P. Bohley, 1977, *The Electrically Small Magnetically-Loaded Multiturn Loop Antenna*, IEEE Transactions on Antennas & Propagation, Vol. AP-25, #4(July), pp. 496-505.

J. Galejs, 1965, '*Admittance of Insulated Loop Antennas in a Dissipative Medium*', IEEE Transactions on Antennas & Propagation, March, pp. 229-235.

R. N. Grubb, P. L. Orswell, and J. H. Taylor, 1976, *Borehole Measurements of conductivity and dielectric constant in the 300kHz to 25MHz Frequency Range*, Radio Science, Vol. 11, No. 4(April), pp.275-283.

R. C. Hansen, 1963,'*Radiation and Reception with Buried and Submerged Antennas*', IEEE Transactions on Antennas & Propagation, May, pp. 207-216.

M. Kazimierczuk, 1983, *Exact analysis of Class E Tuned Power Amplifier with Only One Inductor and One Capacitor in Load Network*, IEEE Journal of Solid-State Circuits, Vol. SC-18, No. 2(April), pp 214-221.

M. B. Kraichman, 1962, '*Impedance of a Circular Loop in an Infinite Conducting Medium*', NBS Journal of Research, Vol.66D, No. 4, July-August, pp. 499-503.

H. L. Krauss, C. W. Bostian, and F. H. Raab, 1980, *Solid State Radio Engineering*, John Wiley & Sons, New York, pp. 433-448.

H. W. March, 1929, *The field of a magnetic dipole in the presence of a conducting sphere*, Bulletin of the American Mathematical Society, Vol. XXXV (July-August) page 455.

H. W. March, 1953, *The field of a magnetic dipole in the presence of a conducting sphere*, Geophysics, Vol. 18, No. 3 (July), pp. 671-684.

R. K. Moore, 1963, '*Effect of a Surrounding Conducting Medium on Antenna Analysis*', IEEE Transactions on Antennas & Propagation, May, pp. 216-225.

G. A. Newman and D. L. Alumbaugh, 1996, *Electromagnetic Modeling of Subsurface 3D Structures*, Proceedings of the 1996 IEEE International Geoscience and Remote Sensing Symposium, Lincoln, Nebraska, May 1996, Vol. IV, pp.1941-1944.

F. H. Raab, 1977, *Idealized Operation of the Class E Tuned Power Amplifier*, IEEE Transactions on Circuits and Systems, Vol. CAS-24, No. 12(December), pp. 725-735.

F. H. Raab, 1978, *Effects of Circuit Variations on the Class E Tuned Power Amplifier*, IEEE Journal of Solid State Circuits, Vol. SC-13, No. 2(April), pp.239-247.

V. H. Rumsey and W. L. Weeks,1956, '*Electrically small, ferrite-loaded Loop Antennas*', IRE Convention Record, Part 1, pp. 165-170.

S. A. Schelkunoff and H. T. Friis, 1952, *Antennas, Theory and Practice*, John Wiley & Sons, New York, pp. 85, 103.

G. S. Smith, 1973, '*A Theoretical and Experimental Study of the Insulated Loop Antenna in a Dissipative Medium*', Radio Science, Vol. 8, N0. 7, July, pp. 711-725,

N. O. Sokal and A. D. Sokal, 1975, *Class E-A New Class of of High-Efficiency Tuned Single-Ended Switching Power Amplifiers*, IEEE Journal of Solid State Circuits, Vol. SC-10, No. 3, June, pp.168-176.

A. Sommerfeld, 1949, *Partial Differential Equations in Physics*, Academic Press, New York, pp. 236-240.

J. A. Stratton, 1941, *Electromagnetic Theory*, McGraw-Hill, New York, pp. 273-276.

J. R. Wait, 1957, *Insulated Loop Antenna Immersed in a Conducting Medium*, NBS Journal of Research, Vol. 59, No. 2, August, pp. 133-137.

J. R. Wait and K. P. Spies, 1964, *A Note on the Insulated Loop Antenna Immersed in a Conducting Medium*, NBS Journal of Research, Vol. 68D, No. 11, November, pp. 1249-1250.

J. R. Wait and D. A. Hill, 1977, *Electromagnetic Fields of a Dipole Source in a Circular Tunnel Containing a Surface Wave Line*, International Journal of Electronics, Vol. 42, No. 4, pp. 377-391.

DISTRIBUTION:

1 Dr. L. G. Stolarczyk
Raton Technology Research
P. O. Box 428
Raton, NM 87740

1 MS 0537 W. H. Hensley, 2344
1 0655 J. C. Bartberger, 5736
1 0701 R. W. Lynch, 6100
1 0705 L. C. Bartel, 6116
15 0705 T. W. H. Caffey, 6116
1 0705 D. L. Alumbaugh, 6116
1 0705 G. A. Newman, 6116
1 0705 M. C. Walck, 6116
1 0860 R. L. Woodfin, 2522
1 0974 E. F. Roseth, 6525
1 1194 L. W. Anderson, 9573
1 1307 M. W. Scott, 1307

1 9018 Central Technical Files, 8940-2
5 0899 Technical Library, 4916
2 0619 Review & Approval Desk, 12690
For DOE/OSTI
1 1380 Technology Transfer, 4212